Determination of α_S using OPAL hadronic event shapes at $\sqrt{s} = 91 - 209$ GeV and resummed NNLO calculations

The OPAL Collaboration

Abstract

Hadronic event shape distributions from e^+e^- annihilation measured by the OPAL experiment at centre-of-mass energies between 91 GeV and 209 GeV are used to determine the strong coupling α_S. The results are based on QCD predictions complete to the next-to-next-to-leading order (NNLO), and on NNLO calculations matched to the resummed next-to-leading-log-approximation terms (NNLO+NLLA). The combined NNLO result from all variables and centre-of-mass energies is

$$\alpha_S(m_{Z^0}) = 0.1201 \pm 0.0008(\text{stat.}) \pm 0.0013(\text{exp.}) \pm 0.0010(\text{had.}) \pm 0.0024(\text{theo.}).$$

while the combined NNLO+NLLA result is

$$\alpha_S(m_{Z^0}) = 0.1189 \pm 0.0008(\text{stat.}) \pm 0.0016(\text{exp.}) \pm 0.0010(\text{had.}) \pm 0.0036(\text{theo.}).$$

The completeness of the NNLO and NNLO+NLLA results with respect to missing higher order contributions, studied by varying the renormalization scale, is improved compared to previous results based on NLO or NLO+NLLA predictions only. The observed energy dependence of α_S agrees with the QCD prediction of asymptotic freedom and excludes the absence of running.

final draft
January 7, 2011

The OPAL Collaboration

G. Abbiendi[2], C. Ainsley[5,u], P.F. Åkesson[7], G. Alexander[21], G. Anagnostou[1], K.J. Anderson[8], S. Asai[22], D. Axen[26], I. Bailey[25,g], E. Barberio[7,o], T. Barillari[31], R.J. Barlow[15], R.J. Batley[5], P. Bechtle[24], T. Behnke[24], K.W. Bell[19], P.J. Bell[1], G. Bella[21], A. Bellerive[6], G. Benelli[4,j], S. Bethke[31], O. Biebel[30], O. Boeriu[9], P. Bock[10], M. Boutemeur[30], S. Braibant[2], R.M. Brown[19], H.J. Burckhart[7], S. Campana[4,x], P. Capiluppi[2], R.K. Carnegie[6], A.A. Carter[12], J.R. Carter[5], C.Y. Chang[16], D.G. Charlton[1], C. Ciocca[2], A. Csilling[28], M. Cuffiani[2], S. Dado[20], M. Dallavalle[2], A. De Roeck[7], E.A. De Wolf[7,r], K. Desch[24], B. Dienes[29], J. Dubbert[30,f], E. Duchovni[23], G. Duckeck[30], I.P. Duerdoth[15], E. Etzion[21], F. Fabbri[2], P. Ferrari[7], F. Fiedler[30], I. Fleck[9], M. Ford[15], A. Frey[7], P. Gagnon[11], J.W. Gary[4], C. Geich-Gimbel[3], G. Giacomelli[2], P. Giacomelli[2], M. Giunta[4,a4], J. Goldberg[20], E. Gross[23], J. Grunhaus[21], M. Gruwé[7], A. Gupta[8], C. Hajdu[28], M. Hamann[24], G.G. Hanson[4], A. Harel[20], M. Hauschild[7], C.M. Hawkes[1], R. Hawkings[7], G. Herten[9], R.D. Heuer[7], J.C. Hill[5], D. Horváth[28,c], P. Igo-Kemenes[10], K. Ishii[22,t], H. Jeremie[17], P. Jovanovic[1], T.R. Junk[6,a3], J. Kanzaki[22,t], D. Karlen[25], K. Kawagoe[22], T. Kawamoto[22], R.K. Keeler[25], R.G. Kellogg[16], B.W. Kennedy[19], S. Kluth[31], T. Kobayashi[22], M. Kobel[3,s], S. Komamiya[22], T. Krämer[24], A. Krasznahorkay Jr.[29,e], P. Krieger[6,k], J. von Krogh[10], T. Kuhl[24], M. Kupper[23], G.D. Lafferty[15], H. Landsman[20], D. Lanske[13,*], D. Lellouch[23], J. Letts[n], L. Levinson[23], J. Lillich[9], S.L. Lloyd[12], F.K. Loebinger[15], J. Lu[26,b], A. Ludwig[3,s], J. Ludwig[9], W. Mader[3,s], S. Marcellini[2], A.J. Martin[12], T. Mashimo[22], P. Mättig[l], J. McKenna[26], R.A. McPherson[25], F. Meijers[7], W. Menges[24], F.S. Merritt[8], H. Mes[6,a], N. Meyer[24], A. Michelini[2], S. Mihara[22,t], G. Mikenberg[23], D.J. Miller[14], W. Mohr[9], T. Mori[22], A. Mutter[9], K. Nagai[12,a2], I. Nakamura[22,t], H. Nanjo[22,v], H.A. Neal[32], S.W. O'Neale[1,*], A. Oh[7], M.J. Oreglia[8], S. Orito[22,*], C. Pahl[31], G. Pásztor[4,a5], J.R. Pater[15], J.E. Pilcher[8], J. Pinfold[27], D.E. Plane[7], O. Pooth[13], M. Przybycień[7,m], A. Quadt[31], K. Rabbertz[7,q], C. Rembser[7], P. Renkel[23], J.M. Roney[25], A.M. Rossi[2], Y. Rozen[20], K. Runge[9], K. Sachs[6], T. Saeki[22,t], E.K.G. Sarkisyan[7,i], A.D. Schaile[30], O. Schaile[30], P. Scharff-Hansen[7], J. Schieck[31,z], T. Schörner-Sadenius[7,y], M. Schröder[7], M. Schumacher[3], R. Seuster[13,f], T.G. Shears[7,h], B.C. Shen[4,*], P. Sherwood[14], A. Skuja[16], A.M. Smith[7], R. Sobie[25], S. Söldner-Rembold[15], F. Spano[8,w], A. Stahl[13], D. Strom[18], R. Ströhmer[30,a1], S. Tarem[20], M. Tasevsky[7,d], R. Teuscher[8,k], M.A. Thomson[5], E. Torrence[18], D. Toya[22], I. Trigger[7,a], Z. Trócsányi[29,e], E. Tsur[21], M.F. Turner-Watson[1], I. Ueda[22], B. Ujvári[29,e], C.F. Vollmer[30], P. Vannerem[9], R. Vértesi[29,e], M. Verzocchi[16], H. Voss[7,p], J. Vossebeld[7,h], C.P. Ward[5], D.R. Ward[5], P.M. Watkins[1], A.T. Watson[1], N.K. Watson[1], P.S. Wells[7], T. Wengler[7], N. Wermes[3], G.W. Wilson[15,j], J.A. Wilson[1], G. Wolf[23], T.R. Wyatt[15], S. Yamashita[22], D. Zer-Zion[4], L. Zivkovic[20]

[1]School of Physics and Astronomy, University of Birmingham, Birmingham B15 2TT, UK
[2]Dipartimento di Fisica dell' Università di Bologna and INFN, I-40126 Bologna, Italy
[3]Physikalisches Institut, Universität Bonn, D-53115 Bonn, Germany

[4] Department of Physics, University of California, Riverside CA 92521, USA
[5] Cavendish Laboratory, Cambridge CB3 0HE, UK
[6] Ottawa-Carleton Institute for Physics, Department of Physics, Carleton University, Ottawa, Ontario K1S 5B6, Canada
[7] CERN, European Organisation for Nuclear Research, CH-1211 Geneva 23, Switzerland
[8] Enrico Fermi Institute and Department of Physics, University of Chicago, Chicago IL 60637, USA
[9] Fakultät für Physik, Albert-Ludwigs-Universität Freiburg, D-79104 Freiburg, Germany
[10] Physikalisches Institut, Universität Heidelberg, D-69120 Heidelberg, Germany
[11] Indiana University, Department of Physics, Bloomington IN 47405, USA
[12] Queen Mary and Westfield College, University of London, London E1 4NS, UK
[13] Technische Hochschule Aachen, III Physikalisches Institut, Sommerfeldstrasse 26-28, D-52056 Aachen, Germany
[14] University College London, London WC1E 6BT, UK
[15] School of Physics and Astronomy, Schuster Laboratory, The University of Manchester M13 9PL, UK
[16] Department of Physics, University of Maryland, College Park, MD 20742, USA
[17] Laboratoire de Physique Nucléaire, Université de Montréal, Montréal, Québec H3C 3J7, Canada
[18] University of Oregon, Department of Physics, Eugene OR 97403, USA
[19] Rutherford Appleton Laboratory, Chilton, Didcot, Oxfordshire OX11 0QX, UK
[20] Department of Physics, Technion-Israel Institute of Technology, Haifa 32000, Israel
[21] Department of Physics and Astronomy, Tel Aviv University, Tel Aviv 69978, Israel
[22] International Centre for Elementary Particle Physics and Department of Physics, University of Tokyo, Tokyo 113-0033, and Kobe University, Kobe 657-8501, Japan
[23] Particle Physics Department, Weizmann Institute of Science, Rehovot 76100, Israel
[24] Universität Hamburg/DESY, Institut für Experimentalphysik, Notkestrasse 85, D-22607 Hamburg, Germany
[25] University of Victoria, Department of Physics, P O Box 3055, Victoria BC V8W 3P6, Canada
[26] University of British Columbia, Department of Physics, Vancouver BC V6T 1Z1, Canada
[27] University of Alberta, Department of Physics, Edmonton AB T6G 2J1, Canada
[28] Research Institute for Particle and Nuclear Physics, H-1525 Budapest, P O Box 49, Hungary
[29] Institute of Nuclear Research, H-4001 Debrecen, P O Box 51, Hungary
[30] Ludwig-Maximilians-Universität München, Sektion Physik, Am Coulombwall 1, D-85748 Garching, Germany
[31] Max-Planck-Institute für Physik, Föhringer Ring 6, D-80805 München, Germany
[32] Yale University, Department of Physics, New Haven, CT 06520, USA

[a] and at TRIUMF, Vancouver, Canada V6T 2A3
[b] now at University of Alberta
[c] and Institute of Nuclear Research, Debrecen, Hungary
[d] now at Institute of Physics, Academy of Sciences of the Czech Republic 18221 Prague,

3

Czech Republic

[e] and Department of Experimental Physics, University of Debrecen, Hungary

[f] now at MPI München

[g] now at Lancaster University

[h] now at University of Liverpool, Dept of Physics, Liverpool L69 3BX, U.K.

[i] now at University of Texas at Arlington, Department of Physics, Arlington TX, 76019, U.S.A.

[j] now at University of Kansas, Dept of Physics and Astronomy, Lawrence, KS 66045, U.S.A.

[k] now at University of Toronto, Dept of Physics, Toronto, Canada

[l] now at Bergische Universität, Wuppertal, Germany

[m] now at University of Mining and Metallurgy, Cracow, Poland

[n] now at University of California, San Diego, U.S.A.

[o] now at The University of Melbourne, Victoria, Australia

[p] now at IPHE Université de Lausanne, CH-1015 Lausanne, Switzerland

[q] now at IEKP Universität Karlsruhe, Germany

[r] now at University of Antwerpen, Physics Department,B-2610 Antwerpen, Belgium; supported by Interuniversity Attraction Poles Programme – Belgian Science Policy

[s] now at Technische Universität, Dresden, Germany

[t] and High Energy Accelerator Research Organisation (KEK), Tsukuba, Ibaraki, Japan

[u] now at University of Pennsylvania, Philadelphia, Pennsylvania, USA

[v] now at Department of Physics, Kyoto University, Kyoto, Japan

[w] now at Columbia University

[x] now at CERN

[y] now at DESY

[z] now at Ludwig-Maximilians-Universität München, Germany

[a1] now at Julius-Maximilians-University Würzburg, Germany

[a2] now at University of Tsukuba, Japan

[a3] now at FERMILAB

[a4] now at Università di Bologna and INFN

[a5] now at University of Geneva

[a6] now at Georg-August University of Göttingen

[*] Deceased

1   Introduction

Events originating from e^+e^- annihilation into quark-antiquark pairs allow precision tests [1–3] of the theory of the strong interaction, Quantum Chromodynamics (QCD) [4–7]. Comparison of observables like jet production rates or event shape variables with theoretical predictions allows the crucial free parameter of QCD – the strong coupling α_S – to be determined. The determination of α_S from many different observables provides an important consistency test of QCD. Recently, significant progress in the theoretical calculation of event shape observables has been made. Next-to-next-to-leading order (NNLO) calculations are now available [8,9] as well as NNLO calculations matched with resummed terms in the next-to-leading-logarithmic-approximation (NLLA) [10].

Measurements of α_S at centre-of-mass-system (c.m.) energies between $\sqrt{s} = 91$ GeV and 206 GeV, using NNLO predictions and ALEPH data, were presented in [11]. This was followed by measurements between $\sqrt{s} = 14$ GeV and $\sqrt{s} = 44$ GeV [12] and between $\sqrt{s} = 91$ GeV and $\sqrt{s} = 206$ GeV [13] based on comparing JADE or ALEPH data with NNLO plus matched NLLA calculations. The strong coupling has also been determined at NNLO from the three-jet rate at LEP [14]. In the present study, the revised NNLO calculations described in [8,9] are used to determine α_S at NNLO and NNLO+NLLA for 13 different energy values between 91 and 209 GeV. The data sample is that of the OPAL Collaboration at LEP. Hadronization corrections are treated in the manner described in [2,11,12,15]. The study is based on the same measurements of event shape variables, the same fit ranges (except for y_{23}^{D} as discussed below), and the same Monte Carlo models for detector and hadronization corrections as those in [15].

The structure of the paper is as follows. In Sect. 2 we give an overview of the OPAL detector, and in Sect. 3 we summarize the data and Monte Carlo samples used. The theoretical background to the work is outlined in Sect. 4. The experimental analysis techniques are explained in Sect. 5, and the measurements are compared with theory in Sect. 6.

2   The OPAL Detector

The OPAL experiment operated from 1989 to 2000 at the LEP e^+e^- collider at CERN. The OPAL detector is described in detail in [16–18]. This analysis mostly makes use of the measurements of energy deposited in the electromagnetic calorimeter and of charged particle momenta in the tracking chambers.

All tracking systems were located inside a solenoidal magnet, which provided a uniform axial magnetic field of 0.435 T along the beam axis. The main tracking detector was the central jet chamber. This device was approximately 4 m long and had an outer radius of about 1.85 m. The magnet was surrounded by a lead glass electromagnetic calorimeter and a sampling hadron calorimeter. The electromagnetic calorimeter consisted of 11704 lead glass blocks, covering 98% of the solid angle. Outside the hadron calorimeter, the detector was surrounded by a system of muon chambers.

3 Data and Monte Carlo Samples

The analysis is based on the same data, Monte Carlo samples, and event selection, as those employed in a previous study [15]. The data were collected at c.m. energies between 91.0 GeV and 208.9 GeV. The data at 91 GeV, on the Z^0 peak, were collected during calibration runs between 1996 and 2000 and have the same conditions of detector configuration, performance and software reconstruction as the higher energy data. The data are grouped into samples with similar c.m. energies, as indicated in Tab. 1. Besides the energy range, mean energy and integrated luminosity, Tab. 1 lists the year(s) of collection and the number of selected hadronic annihilation events for each sample.

Samples of Monte Carlo-simulated events were used to correct the data for experimental acceptance, efficiency and backgrounds. The $e^+e^- \to q\overline{q}$ process was simulated at $\sqrt{s} = 91.2$ GeV using JETSET 7.4 [19], and at higher energies using $\mathcal{KK}$2f 4.01 or $\mathcal{KK}$2f 4.13 [20, 21] with hadronization performed using PYTHIA 6.150 or PYTHIA 6.158 [19]. Corresponding samples of HERWIG 6.2 [22, 23] or $\mathcal{KK}$2f events with HERWIG 6.2 hadronization were used for systematic checks. Four-fermion background processes were simulated using grc4f 2.1 [24], KORALW 1.42 [25] with grc4f [24] matrix elements, with hadronization performed using PYTHIA. The above samples, generated at each energy point studied, were processed through a full simulation of the OPAL detector [26] and reconstructed in the same manner as the data. In addition, when correcting for the effects of hadronization, large samples of generator-level Monte Carlo events were employed, using the parton shower models PYTHIA 6.158, HERWIG 6.2 and ARIADNE 4.11 [27].

Each of these models used for the description of hadronization and detector response contains a number of tunable parameters. These parameters were adjusted to describe previously published OPAL data at $\sqrt{s} \sim 91$ GeV as discussed in [28] for PYTHIA/ JETSET and in [29] for HERWIG and ARIADNE.

4 Theoretical Background

4.1 Event Shape Distributions

The properties of hadronic events can be described by event shape observables. The event shape observables used for this analysis are thrust $(1 - T)$ [30, 31], heavy jet mass (M_H) [32], wide and total jet broadening $(B_W$ and $B_T)$ [33], C-Parameter (C) [34–36] and the transition value between 2 and 3 jet configurations defined using the Durham jet algorithm (y_{23}^D) [37].

In the following, the symbol y is used to refer to any of the variables $1 - T$, M_H, B_T, B_W, C or y_{23}^D. Event shape variables characterize the main features of the distribution of momentum in an event. Larger values of y correspond to the multi-jet region dominated by the radiation of hard gluons. Smaller values of y correspond to the two-jet region with only soft and collinear radiation.

4.2 QCD Calculations

QCD predictions for the distribution of event shape observables in e^+e^- annihilations are now available to $\mathcal{O}(\alpha_S^3)$ (NNLO) [8, 9]. In the case where the renormalization scale μ_R equals the physical scale Q identified with $\sqrt{s}$, the predictions are:

$$\frac{1}{\sigma}\frac{\mathrm{d}\sigma}{\mathrm{d}y}\bigg|_{\mathcal{O}(\alpha_S^3)} = \frac{\mathrm{d}A}{\mathrm{d}y}\hat{\alpha}_S + \frac{\mathrm{d}B}{\mathrm{d}y}\hat{\alpha}_S^2 + \frac{\mathrm{d}C}{\mathrm{d}y}\hat{\alpha}_S^3 \tag{1}$$

with $\hat{\alpha}_S = \alpha_S(\mu_R)/(2\pi)$. The coefficient distributions for the leading order (LO) $\mathrm{d}A/\mathrm{d}y$, next-to-leading order (NLO) $\mathrm{d}B/\mathrm{d}y$ and NNLO $\mathrm{d}C/\mathrm{d}y$ terms were provided to us by the authors of [8]. The normalization to the total hadronic cross section and the terms generated by variation of the renormalization scale parameter $x_\mu = \mu_R/Q$ are implemented according to the prescription of [8].

In the two-jet (low y) region, the effect of soft and collinear emissions introduces large logarithmic effects depending on $L = \log(1/y)$. For the $(1-T)$, M_H, B_T, B_W, C and y_{23}^D distributions, the leading and next-to-leading logarithmic terms can be resummed up to infinite order in perturbation theory [38]. This is referred to as the next-to-leading-logarithmic approximation (NLLA). The most complete calculations of event shape observables are obtained from combining (matching) the $\mathcal{O}(\alpha_S^3)$ and NLLA calculations, taking care not to double count terms that are in common between them.

The matching is not unique. In the so-called $\ln R$ matching scheme, the NNLO+NLLA expression for the logarithm of the cumulative distribution $R(y) = \int_0^y \mathrm{d}y'(1/\sigma)\mathrm{d}\sigma/\mathrm{d}y'$ is [10]

$$
\begin{aligned}
\ln\ (R\,(y,\hat{\alpha}_S)) &= L\,g_1\,(\hat{\alpha}_S L)\ +\ g_2\,(\hat{\alpha}_S L) \\
&+\ \hat{\alpha}_S\left(A\,(y) - G_{11}L - G_{12}L^2\right) \\
&+\ \hat{\alpha}_S^2\left(B\,(y) - \frac{1}{2}A^2\,(y) - G_{22}L^2 - G_{23}L^3\right) \\
&+\ \hat{\alpha}_S^3\left(C\,(y) - A\,(y)\,B\,(y) + \frac{1}{3}A^3\,(y) - G_{33}L^3 - G_{34}L^4\right).
\end{aligned}
\tag{2}
$$

The functions g_1 and g_2 represent the resummed leading and next-to-leading logarithmic terms while the G_{ij} are matching coefficients. The coefficient functions A, B and C are related to the differential coefficients in (1) by integration, e.g. $A(y) = \int_0^y \mathrm{d}y'\frac{\mathrm{d}A(y')}{\mathrm{d}y'}$. Since α_S in the NNLO and NLLA terms are assumed to be the same, there is only one renormalization scale. The NLLA terms introduce a further arbitrariness in the choice of a logarithmic rescaling variable x_L, see [15].

The theoretical calculations provide distributions at the level of quarks and gluons, the so-called parton-level. Monte Carlo-based distributions calculated using the final-state partons after termination of the parton showering in the models are also said to be at the parton-level. In contrast, the data are corrected to the hadron-level, i.e. they correspond to the distributions of the stable particles in the event as explained in Sect. 5.2. To compare the QCD predictions with measured event shape distributions these predictions are corrected from the parton to the hadron level. The corrections are based on large samples of typically 10^7 events generated with the parton-shower Monte Carlo programs

PYTHIA (used by default), HERWIG and ARIADNE (used to evaluate systematic uncertainties). The corrections are defined by the ratio of the Monte Carlo distributions at the hadron and parton levels and are applied as multiplicative corrections to the theoretical predictions.

We compare the parton-level calculations of the Monte Carlo generators with the QCD calculations in NNLO+NLLA with $\alpha_S(m_{Z^0}) = 0.118$, $x_\mu = 1.0$ and $x_L = 1.0$ at $\sqrt{s} = 91$ GeV, see Fig. 1 and [12]. The dashed line shows the deviation from one of the ratio between the Pythia prediction at the parton level and the NNLO+NLLA calculation. The dotted (dash-dotted) line shows the corresponding result from Herwig (Ariadne). The solid lines, symmetric about zero, show the maximum difference between any pair of the Monte Carlo models, which are seen to be of similar size to the differences between the generators and the NNLO+NNLA calculation. Therefore we consider that the MC simulations adequately account for the hadronization correction to the calculations.

The model dependence of the hadronization correction is included as a systematic uncertainty as described below.

5 Experimental Procedure

The data used in the present paper are identical to those presented in [15, 39, 40]. For completeness and to facilitate the discussion of systematic uncertainties, we give a brief summary of the analysis procedure below.

5.1 Event Selection

The event selection procedure is described in [15]. This procedure selects well-measured hadronic event candidates, removes events with a large amount of initial-state radiation (ISR) at 130 GeV and above, and removes four-fermion background events above the W^+W^- production threshold of 160 GeV.

5.2 Corrections to the Data

For each accepted event, the value of each event shape observable is computed. A standard algorithm [41] is applied to mitigate the double-counting of energy between the tracking chambers and calorimeter. To correct for background contributions, the expected number of residual four-fermion events b_i is subtracted from the number of data events N_i in each bin i of each distribution. Simple bin-by-bin corrections are applied to account for detector acceptance, resolution, and the effects of residual ISR. We examine the Monte Carlo predictions for the event shape variables at two levels: the detector level, which includes simulation of the detector and the same analysis procedures as applied to the data, and the hadron level, which uses stable particles[1] only, assumes perfect reconstruction of the particle momenta, and requires the hadronic c.m. energy $\sqrt{s'}$ to satisfy $\sqrt{s} - \sqrt{s'} < 1$ GeV. The ratio of the hadron- to the detector-level prediction for each bin, α_i, is used as the correction factor for the data, yielding the corrected bin content $\widetilde{N}_i = \alpha_i(N_i - b_i)$.

---

[1]For this purpose, all particles having proper lifetimes greater than 3×10^{-10} s are regarded as stable.

This corrected hadron-level distribution is then normalized by the total number of events $N = \sum_k \widetilde{N}_k$ and bin width W_i: $P_i = \widetilde{N}_i/(NW_i)$.

5.3 Systematic uncertainties

To evaluate systematic uncertainties, the analysis is repeated after modifying the selection or correction procedures. The event and track selection cuts are varied within the ranges of values suggested in [15]. The Monte Carlo model employed to calculate the detector correction is altered, and the cross section used in the subtraction of four-fermion events is varied by $\pm 5\%$. In each case, the difference in each bin with respect to the standard analysis is taken as a contribution to the systematic uncertainty.

6 Determinations of α_S

6.1 Fit procedure

The strong coupling α_S is determined using a minimum-χ^2 fit, comparing theory with each of the measured event shape distributions at the hadron level. A χ^2 value is calculated at each c.m. energy:

$$\chi^2 = \sum_{i,j}^{n} (P_i - t_i(\alpha_S))(V^{-1})_{ij}(P_j - t_j(\alpha_S)) \tag{3}$$

where i, j include the bins within the fit range of the event shape distribution, P_i is the measured value in the ith bin, $t_i(\alpha_S)$ is the QCD prediction for the ith bin corrected for hadronization effects, and V^{-1} is the inverse of the statistical covariance matrix V^{stat} of the values P_i. The QCD prediction is obtained by integrating the result in (1) over the bin width, and then applying the hadronization correction. The χ^2 value is minimized with respect to α_S with the renormalization scale factor x_μ and the rescaling variable x_L set to 1. The evolution of the strong coupling α_S as a function of the renormalization scale is implemented to three-loop order [42]. Since the c.m. energy range considered here does not cross flavour thresholds, no significant uncertainties are introduced by the evolution of α_S. Separate fits are performed to each of the six observables at each c.m. energy value.

To account for correlations between bins in the computation of χ^2, the statistical covariance matrix V_{ij}^{stat} is calculated following the approach described in [15]:

$$\begin{aligned} V_{ij}^{\text{stat}} &= \sum_k \frac{\partial P_i}{\partial N_k}\frac{\partial P_j}{\partial N_k}N_k \\ &= \frac{1}{N^4}\sum_k \alpha_k^2 N_k \left(N\delta_{ik} - \widetilde{N}_i\right)\left(N\delta_{jk} - \widetilde{N}_j\right) . \end{aligned} \tag{4}$$

where δ_{ik} is the Kronecker delta function, and the other terms are defined in Sect. 5.2.

To test our procedure, we verified that we are able to reproduce the fit results from [15, 43] using NLO+NLLA predictions within typically 0.5%.

The fit ranges are chosen as in [15,44] and correspond to regions where the corrections of the data and of the parton level theory to the hadron level are both reasonably small and where the NLO+NLLA fit results are stable under small variations of the fit range. The relevant calculations in the two-jet region are the NLLA terms, which are identical in the present study and [15]. The NNLO prediction for y_{23}^{D} is given in bins of $-\ln y_{23}^{\mathrm{D}}$. The transformation to bins of y_{23}^{D} produces precision problems for small values of y_{23}^{D}. Therefore we use a more restrictive fit range for y_{23}^{D} than in [15], which approximately matches the range in [12]: the lower bound is 0.012 rather than 0.0023.

The fit ranges are shown in Tab. 2. In the resummation of log-enhanced terms, the leading log term of $\mathrm{d}A/\mathrm{d}y$ is $\ln(y)/y$. At y values equal to the lower limit y_0, the value of $\hat{\alpha}_{\mathrm{S}}\ln(y_0)/y_0$ is still of the order of one for $\alpha_{\mathrm{S}}(m_{\mathrm{Z}^0}) = 0.118$ and $91 \leq \sqrt{s} \leq 207$ GeV. Thus the fit ranges are also suitable for pure NNLO analysis.

Previously measured event shape distributions are published [15] only in the energy ranges as separated by horizontal lines in Tab. 1. We perform fits to extract α_{S} at all of the energy points[2] shown in Tab. 1 column 2. We average over the larger energy ranges only for purposes of presentation.

The detector correction factors are typically between 0.9 and 1.5 within the fit ranges. For energies above 189 GeV, which have low statistics, the corrections exceed 2.0 in the multi-jet regions. The maximum correction of 4.8 occurs for the $1 - T$ distribution at 207 GeV. The variable with the least variation in the size of its hadronization correction, and with hadronization corrections closest to one, is y_{23}^{D}.

The statistical uncertainty of α_{S} is given by the variation required to increase χ^2 by one unit from its minimum. The systematic uncertainties account for experimental effects, the hadronization correction procedure and uncertainties of the theory. The three sources of systematic uncertainty are added in quadrature to the statistical uncertainty to define the total uncertainty. Below, we describe the evaluation of systematic uncertainties. For each variant of the analysis, the corresponding distribution is fitted to determine α_{S}, and the difference with respect to the value of α_{S} from the default analysis is taken as a systematic uncertainty contribution.

Experimental Uncertainties: These are assessed as described in Sect. 5.3.

Hadronization: For the default analysis, PYTHIA is used to evaluate hadronization corrections (Sect. 4.2). As systematic variations, HERWIG and ARIADNE are used instead. The larger of the deviations is taken as the systematic uncertainty. It was observed in [45, 46] that systematic uncertainties determined from the differences between the PYTHIA, HERWIG, and ARIADNE models are generally much larger than those that arise from varying the parameters of a given model.

Theoretical Uncertainties: The theoretical calculation of event shape observables is a finite power series in α_{S}. The uncertainties originating from missing higher order terms are assessed by changing the renormalization scale factor to $x_\mu = 0.5$ and $x_\mu = 2.0$. The rescaling variable is set to $x_L = 2/3$ and $x_L = 3/2$ ($x_L = 4/9$ and $x_L = 9/4$ in case of y_{23}^{D}) [15]. The largest deviation with respect to the standard

---

[2]This allows the use of the event shape covariance matrices which are energy dependent and have been calculated separately for each energy point.

analysis is taken as the systematic uncertainty. A variation of the matching scheme is not studied because R-matching is not available for NNLO+NLLA. The matching scheme was not an important source of uncertainty in studies of α_S based on NLO+NLLA calculations.

6.2 Results from NNLO Fits

The results of the NNLO fits are summarised in Tab. 3. In order to clarify the presentation, the α_S values from 130 and 136 GeV are combined[3], and likewise the values from 161 to 183 GeV, and from 189 GeV and above. These three ranges of c.m. energies, which correspond to luminosity weighted mean energies of 133.1, 177.4 and 197.0 GeV, respectively, cover sufficiently small ranges of $\sqrt{s}$ that only small variations of α_S occur within each range.

Figs. 2, 3 and 4 show the $1 - T$, M_H, B_T, B_W, C and y_{23}^D event shape distributions together with the NNLO fit results for the 91.3 and 206.6 GeV energy points. All event shape distributions are described reasonably well by the fitted predictions. The χ^2/d.o.f. values, which are large for the data at the Z^0 peak because they are based on statistical uncertainties only, range from 0.03 for y_{23}^D at $\sqrt{s} = 191.6$ GeV to 228 for B_T at $\sqrt{s} = 91.3$ GeV. The uncertainties at this point are dominated by the experimental systematic uncertainties (discussed below). To check how the inclusion of the experimental errors in the fits reduces the large χ^2 values, an alternative χ^2 value is defined as follows. An estimate of the experimental systematic covariance is added to the statistical covariance (4),

$$V_{ij}^{\text{total}} = V_{ij}^{\text{stat}} + \min(\sigma_{\exp,i}^2, \sigma_{\exp,j}^2), \tag{5}$$

where $\sigma_{\exp,i}$ is the experimental systematic uncertainty at bin i. Tab. 4 shows the fit results at 91 GeV. The fit results are in general not compatible within the combined statistical and experimental errors with the results when only the statistical covariance is used. These χ^2/d.o.f. values are smaller than those from employing the statistical covariances, however they still range up to 62 for B_T. We return to this issue when we discuss the NNLO+NLLA fits below.

The results for α_S from the different event shape variables are remarkably consistent with each other, for each c.m. energy, as seen from Tabs. 10, 11 (but not in the case of the modified fit procedure whose results are shown in Tab. 4). We find root-mean-square (r.m.s.) values for $\alpha_S(\sqrt{s})$ between 0.0012 at 183 GeV and 0.0044 at 202 GeV. The variations in α_S between the different variables are comparable to the total systematic uncertainties. The values of α_S are significantly larger at 91 GeV than at higher energies, providing evidence for the running of α_S. Theoretical uncertainties dominate at the Z^0 peak (except for y_{23}^D), where the statistical uncertainties are small. Similarly, statistical uncertainties are small at 189 GeV where there is a relatively large data sample. Statistical uncertainties dominate at 130, 161 and 172 GeV, where the data samples are smaller. Experimental systematic uncertainties are small at 91 GeV and larger at higher $\sqrt{s}$ where

---

[3]This combination is performed assuming minimum overlap correlation of the experimental uncertainties at the different c.m. energy points. The procedure includes a correction for the running of $\alpha_S(\sqrt{s})$ to the luminosity weighted mean energy.

uncertainties from subtraction of ISR and four fermion events contribute more strongly. For completeness, the fit results for all energy points are given separately in App. A.

6.3 Results from NNLO+NLLA Fits

The results of the NNLO+NLLA fits are shown in Figs. 2, 3 and 4 and listed in Tab. 5. The calculations fit the data better than the pure NNLO calculations at small values of the variables. The values of $\chi^2/\text{d.o.f.}$ are smaller on average than for the NNLO fits, especially at 91 GeV, indicating better consistency with the data. The r.m.s. values of $\alpha_S(\sqrt{s})$ vary between 0.0017 at $\sqrt{s} = 205$ GeV and 0.0051 at $\sqrt{s} = 202$ GeV, i.e. the scatter of individual results is essentially the same as for the NNLO analysis. The pattern of statistical, experimental, and hadronization uncertainties is the same as for the NNLO fits discussed above. At most energy points the theory error results from the x_L variation for M_H, B_W, y_{23}^D, and from the x_μ variation for $1 - T$, B_T, C. Compared with the NNLO analysis the values of α_S are lower by 0.4% on average, and the theoretical uncertainties are higher by 33%. Larger scale uncertainties are expected to arise at 91 GeV when the NLLA terms are added to the NNLO terms [10, 13, 47], because the NNLO calculation compensates for the variation of the renormalization scale in two loops, while the NLLA term compensates for the variation in only one loop. The difference we observe between α_S in the NNLO and NNLO+NLLA studies is smaller than the corresponding difference observed between the NLO and NLO+NLLA studies (Sect. 6.5), as predicted in [10]. This difference is also smaller than that observed at lower energies [12], as expected from the energy evolution of α_S.

The fit results at 91 GeV employing the total covariance (5) are shown in Tab. 6. Unlike the case of pure NNLO, the fit results are compatible with the results based on only the statistical covariance within the combined statistical and experimental systematic uncertainties. The $\chi^2/\text{d.o.f.}$ values are of the order of 1. For a reasonable description of the data by the theory predictions, inclusion of the resummed logarithmic terms (NLLA) is seen to be important. As the covariance (5) is only an approximation, we do not use the fit values or errors further.

6.4 Combination of Results

The results obtained at each energy point for the six event shape observables are combined using uncertainty-weighted averaging as in [2,15,48,49]. The statistical correlations between the six event shape observables are estimated at each energy point from fits to hadron-level distributions derived from 50 statistically-independent Monte Carlo samples. The experimental uncertainties are determined assuming that the smaller of a pair of correlated experimental uncertainties gives the size of the fully correlated uncertainty. The minimum overlap assumption results in a conservative estimate of the total uncertainty. The hadronization and theoretical systematic uncertainties are evaluated by repeating the combination with changed input values, i.e. using a different hadronization model or the different value of x_μ or x_L that yields the maximum deviation. The results are given in Tab. 7 and shown for the NNLO+NLLA analysis in Fig. 5. Also shown is a comparison with the results of a NNLO+NLLA analysis at lower energy from the JADE

Collaboration [12].

To study the compatibility of our data with the QCD prediction for the evolution of the strong coupling with c.m. energy we repeat the combinations with or without evolution of the combined results to the common scale, setting the theory uncertainties to zero since these uncertainties are highly correlated between energy points. We assume the hadronization uncertainties to be partially correlated. The χ^2 probability of the average for a running (constant) coupling in the NNLO+NLLA study is 0.59 (6×10^{-13}). The corresponding result for the NNLO study is 0.56 (2×10^{-6}). We interpret this as clear evidence, from OPAL data alone, for the running of α_S in the manner predicted by QCD.

We evolve the results in Tab. 7 with $\sqrt{s} > m_{Z^0}$ to a common scale m_{Z^0} using the QCD formula for the running of α_S. The results are then combined using the uncertainty-weighted averaging procedure mentioned above. The results are shown in Tab. 8 for the NNLO and NNLO+NLLA analyses. The consistency between these values and the results from 91 GeV (Tab. 7) demonstrates the compatibility of the data with the running predicted by QCD. The high energy data have smaller theoretical and hadronization uncertainties, and therefore complement the statistically superior 91 GeV data.

The values of $\alpha_S(m_{Z^0})$ obtained from combining all energy points are also given in Tab. 8. The resulting values of $\alpha_S(m_{Z^0}) = 0.1201 \pm 0.0031$ from the NNLO study, and $\alpha_S(m_{Z^0}) = 0.1189 \pm 0.0041$ from the NNLO+NLLA study, are consistent with the world average [50] (0.1184 ± 0.0007), recent NNLO analyses of JADE [12] (0.1172 ± 0.0051) and ALEPH [11] (0.1240 ± 0.0033) data, our previous study [15] based on NLO+NLLA calculations (0.1191 ± 0.0047) and the study [13] of ALEPH data using NNLO+NLLA (0.1224 ± 0.0039). The total uncertainties of 2.6% and 3.4% for $\alpha_S(m_{Z^0})$ place these measurements amongst the most precise determinations of α_S available.

After running the fit results for $\alpha_S(\sqrt{s})$ for each observable to the common reference scale m_{Z^0}, we combine the results for a given observable to a single value. We use the same method as above and obtain the results for $\alpha_S(m_{Z^0})$ shown in Tab. 9. These results demonstrate that the measurements from the different observables are far from compatible with each other when only statistical uncertainties are considered, but are consistent with a common mean when the systematic uncertainties are included, neglecting their correlation. The r.m.s. values of the results for $\alpha_S(m_{Z^0})$ are 0.0013 for the NNLO analysis and 0.0026 for the NNLO+NLLA analysis; both values lie within the range of the uncertainty for the corresponding combined result shown in Tab. 8. Fig. 6 displays the combined α_S result for each observable. Results from NLO and NLO+NLLA studies, discussed below, are also shown. Combining the NNLO or NNLO+NLLA results of Fig. 6 to obtain an overall value for α_S, or evolving each event shape measurement from each energy to the reference scale and then combining, yields the same result as given by the corresponding measurement in Tab. 8 to within $\Delta\alpha_S(m_{Z^0}) = 0.0003$.

6.5 Comparison with NLO and NLO+NLLA fits

To compare our results with previous α_S measurements, the fits to the event shape distributions are repeated with NLO predictions and with NLO predictions combined with resummed NLLA with the modified $\ln R$-matching scheme (NLO+NLLA), both with $x_\mu = 1$. The NLO+NLLA calculations with the modified $\ln R$-matching scheme were the

standard of the analyses at the time of termination of the LEP experiments [15,49,51,52]. The fit ranges and procedures for the evaluation of systematic uncertainties are the same as those used above for the NNLO and NNLO+NLLA studies and thus differ somewhat from the previously published results [15,53].

The combination of the fits using NLO predictions yields $\alpha_S(m_{Z^0}) = 0.1261$ ±0.0011(stat.) ± 0.0024(exp.) ± 0.0007(had.) ± 0.0066(theo.) while the combination of NLO+NLLA results yields $\alpha_S(m_{Z^0}) = 0.1173 \pm0.0009$(stat.)$\pm0.0020$(exp.)$\pm0.0008$(had.) ±0.0055(theo.). These results are shown by the corresponding shaded bands in Fig. 6. The result obtained with the NLO+NLLA prediction is consistent with the NNLO and NNLO+NLLA analyses, but the theory uncertainties are larger by a factor of 2.3 and 1.5 respectively. The analysis using NLO predictions gives theoretical uncertainties larger by a factor of 2.8 and 1.8, and the value for $\alpha_S(m_{Z^0})$ is larger compared to the NNLO or NNLO+NLLA results. It has been observed previously that values for α_S from NLO analyses with $x_\mu = 1$ are large in comparison with most other analyses [54]. The NLO+NLLA analysis yields a smaller value of $\alpha_S(m_{Z^0})$ compared to the NLO result, and the NNLO+NLLA analysis a smaller one compared to NNLO. The difference between the NNLO+NLLA and NNLO results is smaller than the difference between those of the NLO+NLLA and NLO fits because a larger part of the NLLA terms is included in the NNLO calculations.

6.6 Renormalization Scale Dependence

To assess the dependence of α_S on the choice of the renormalization scale, the fits to distributions of the six event shape variables are repeated using NNLO, NNLO+NLLA, NLO and NLO+NLLA predictions with $0.1 < x_\mu < 10$. As an example, α_S and the χ^2/d.o.f. for the C variable at $\sqrt{s} = 91$ GeV are shown as a function of x_μ in Fig. 7. The smallest χ^2/d.o.f. values for the fixed order calculations arise at the smallest scales, while with the NLLA calculations smaller χ^2/d.o.f. values occur nearer the physical scale $\sqrt{s}$, i.e. $x_\mu=1$. Near this scale, smaller χ^2/d.o.f. values are observed with the NNLO curves than with the respective NLO curves.

The NLO calculation yields a larger value of α_S than the other calculations for $x_\mu > 0.2$. The $\alpha_S(m_{Z^0})$ values using the NLO+NLLA, NNLO and NNLO+NLLA calculations cross near the natural[4] choice of the renormalization scale $x_\mu = 1$. The NLLA terms at $x_\mu = 1$ averaged over the fit range are almost identical to the $\mathcal{O}(\alpha_S^3)$-terms in the NNLO calculation. A similar behaviour can be observed for $1 - T$ and B_T.

7 Summary and conclusions

In this paper we present determinations of the strong coupling α_S using event shape observable distributions at c.m. energies between 91 and 209 GeV. Fits using NNLO and combined NNLO+NLLA predictions are used to extract α_S. Combining the results from the NNLO fits to the six event shape observables $1 - T$, M_H, B_W, B_T, C and y_{23}^D at the

---

[4]The terms inducing the renormalization scale dependence resemble terms of higher order in α_S weighted with $\ln x_\mu$.

thirteen OPAL energy points yields

$$\alpha_S(m_{Z^0}) = 0.1201 \pm 0.0008(\text{stat.}) \pm 0.0013(\text{exp.}) \pm 0.0010(\text{had.}) \pm 0.0024(\text{theo.}),$$

with a total uncertainty on $\alpha_S(m_{Z^0})$ of 2.6%. Combining the results from the NNLO+NLLA fits yields

$$\alpha_S(m_{Z^0}) = 0.1189 \pm 0.0008(\text{stat.}) \pm 0.0016(\text{exp.}) \pm 0.0010(\text{had.}) \pm 0.0036(\text{theo.}),$$

with a total uncertainty of 3.4%. This result supersedes that presented in [15] because it is based on more complete theoretical predictions while using the same experimental data and procedures. The variations between the combined results for α_S at the different energies are consistent with the running of α_S as predicted by QCD and exclude the absence of running. The α_S results we find for all 13 energy points are given in Tabs. 10-15, for the NNLO, NNLO+NLLA, and NLO+NLLA calculations.

The investigation of the renormalization scale dependence of $\alpha_S(m_{Z^0})$ shows a reduced dependence on x_μ when NNLO or NNLO+NLLA predictions are used, compared to analyses with NLO or NLO+NLLA predictions. The more complete NNLO or NNLO+NLLA QCD predictions thus lead to smaller theoretical uncertainties in our analysis. Adding the NLLA terms to the NNLO predictions significantly improves the description of the data. The standard procedure to quantify theoretical uncertainties leads, however, to somewhat larger uncertainties in most of the NNLO+NLLA fits.

Acknowledgements

References

[1] O. Biebel, Phys. Rept. **340**, 165 (2001)

[2] S. Kluth, Rept. Prog. Phys **69**, 1771 (2006)

[3] G. Dissertori, I.G. Knowles, M. Schmelling, International Series of Monographs on Physics **115** (Clarendon Press, Oxford, 2003)

[4] H. Fritzsch, M. Gell-Mann, H. Leutwyler, Phys. Lett. B **47**, 365 (1973)

[5] D. Gross, F. Wilczek, Phys. Rev. Lett. **30**, 1343 (1973)

[6] D. Gross, F. Wilczek, Phys. Rev. D **8**, 3633 (1973)

[7] H. Politzer, Phys. Rev. Lett. **30**, 1346 (1973)

[8] A. Gehrmann-De Ridder, T. Gehrmann, E. W. N. Glover, G. Heinrich, JHEP **12**, 094 (2007)

[9] S. Weinzierl, Phys. Rev. Lett. **101**, 162001 (2008)

[10] T. Gehrmann, G. Luisoni, H. Stenzel, Phys. Lett. B **664**, 265 (2008)

[11] G. Dissertori et al., JHEP **02**, 040 (2008)

[12] JADE Coll., S. Bethke, S. Kluth, C. Pahl, J. Schieck, Eur. Phys. J. C **64**, 351 (2009)

[13] G. Dissertori et al., JHEP **08**, 036 (2009)

[14] G. Dissertori et al., Phys. Rev. Lett. **104**, 072002 (2010)

[15] OPAL Coll., G. Abbiendi et al., Eur. Phys. J. C **40**, 287 (2005)

[16] OPAL Coll., K. Ahmet et al., Nucl. Instrum. and Methods A **305**, 275 (1991)

[17] OPAL Coll., S. Anderson et al., Nucl. Instrum. and Methods A **403**, 326 (1998)

[18] OPAL Coll., G. Aguillion et al., Nucl. Instrum. and Methods A **417**, 266 (1998)

[19] T. Sjöstrand, Comput. Phys. Commun. **82**, 74 (1994)

[20] S. Jadach, B. Ward, Z. Wąs, Phys. Lett. B **449**, 97 (1999)

[21] S. Jadach et al., Comput. Phys. Commun. **130**, 260 (2000)

[22] G. Marchesini et al., Comput. Phys. Commun. **67**, 465 (1992)

[23] G. Corcella et al., JHEP **01**, 010 (2001)

[24] J. Fujimoto et al., Comput. Phys. Commun **100**, 128 (1997)

[25] S. Jadach et al., Comput. Phys. Commun **119**, 272 (1999)

[26] OPAL Coll., J. Allison et al., Nucl. Instrum. Methods A **317**, 47 (1992)

[27] L. Lönnblad, Comput. Phys. Commun **71**, 15 (1992)

[28] OPAL Coll., G. Alexander et al., Z. Phys. C **69**, 543 (1996)

[29] OPAL Coll., G. Abbiendi et al., Eur. Phys. J. C **35**, 293 (2004)

[30] S. Brandt, C. Peyrou, R. Sosnowski, A. Wroblewski, Phys. Lett. **12**, 57 (1964)

[31] E. Fahri, Phys. Rev. Lett. **39**, 1587 (1977)

[32] T. Chandramohan, L. Clavelli, Nucl. Phys. B **184**, 365 (1981)

[33] S. Catani, G. Turnock, B. Webber, Phys. Lett. B **295**, 269 (1992)

[34] G. Parisi, Phys. Lett. B **74**, 65 (1978)

[35] J. Donoghue, F. Low, S. Pi, Phys. Rev D **20**, 2759 (1979)

[36] R. Ellis, D. Ross, A. Terrano, Nucl. Phys. B **178**, 421 (1981)

[37] S. Catani et al., Phys. Lett. B **269**, 432 (1991)

[38] M. Dasgupta, G. Salam, J. Phys. G **30**, R143 (2004)

[39] OPAL Coll., G. Abbiendi et al., Eur. Phys. J. C **45**, 547 (2006)

[40] OPAL Coll., G. Abbiendi et al., Eur. Phys. J. C **47**, 295 (2006)

[41] OPAL Coll., G. Abbiendi et al., Eur. Phys. J. C **26**, 479 (2003)

[42] R. Ellis, W. Stirling, B. Webber, Cambridge Monographs on Particle Physics, Nuclear Physics and Cosmology **8** (1996), Cambridge University Press

[43] M. Ford, PhD thesis, arXiv:hep-ex/0405054 (2004), University of Cambridge

[44] OPAL Coll., G. Abbiendi et al., Eur. Phys. J. C **16**, 185 (2000)

[45] R.W.L. Jones, M. Ford, G.P. Salam, H. Stenzel, D. Wicke, J. High Energy Phys. **12**, 007 (2003)

[46] P. A. Movilla Fernández, Ph.D. thesis, RWTH Aachen (2003). http://nbn-resolving.de/urn:nbn:de:hbz:82-opus-4836

[47] T. Gehrmann, G. Luisoni, H. Stenzel, arXiv:0810.3599, to appear in High Energy Physics ICHEP 2008, Proceedings of the 34th International Conference (2008)

[48] R. W. L. Jones, Nucl. Phys. Proc. Suppl. **133**, 13 (2004)

[49] ALEPH Coll., A. Heister et al., Eur. Phys. J. C **35**, 457 (2004)

[50] S. Bethke, Eur. Phys. J. C **64**, 689 (2009)

[51] L3 Coll., P. Achard et al., Phys. Rept. **399**, 71 (2004)

[52] DELPHI Coll., J. Abdallah et al., Eur. Phys. J. C C **37**, 1 (2004)

[53] OPAL Coll., P. Acton et al., Z. Phys. C **59**, 1 (1993)

[54] OPAL Coll., P. Acton et al., Z. Phys. C **55**, 1 (1992)

Table 1: Year of data collection, energy range, mean c.m. energy, integrated luminosity $\mathcal{L}$ and numbers of selected events for each OPAL data sample used in this analysis, see also [15]. The horizontal lines divide the data into four energy ranges used for presentation purposes.

Year	Range of $\sqrt{s}$ [GeV]	Mean $\sqrt{s}$ [GeV]	$\mathcal{L}$ [pb^{-1}]	Selected events
1996, 2000	91.0—91.5	91.3	14.7	395695
1995, 1997	129.9—130.2	130.1	5.31	318
1995, 1997	136.0—136.3	136.1	5.95	312
1996	161.2—161.6	161.3	10.06	281
1996	170.2—172.5	172.1	10.38	218
1997	180.8—184.2	182.7	57.72	1077
1998	188.3—189.1	188.6	185.2	3086
1999	191.4—192.1	191.6	29.53	514
1999	195.4—196.1	195.5	76.67	1137
1999, 2000	199.1—200.2	199.5	79.27	1090
1999, 2000	201.3—202.1	201.6	37.75	519
2000	202.5—205.5	204.9	82.01	1130
2000	205.5—208.9	206.6	138.8	1717

Table 2: Fit ranges at all c.m. energies.

$1 - T$	M_{H}	B_{T}
0.05–0.30	0.17–0.45	0.075–0.25
B_{W}	C	y_{23}^{D}
0.05–0.20	0.18-0.60	0.012–0.13

Table 3: Measurements of α_S using NNLO predictions and event shape distributions in four ranges of c.m. energy: at 91.3 GeV, 133.1 GeV, 161–183 GeV (177.4 GeV on average) and 189–209 GeV (197.0 GeV on average).

$\sqrt{s}$ [GeV]	Obs.	$\alpha_S(\sqrt{s})$	±stat.	±exp.	±had.	±theo.	±tot.
91.3	$1-T$	0.1220	0.0002	0.0011	0.0030	0.0042	0.0053
91.3	M_H	0.1228	0.0002	0.0008	0.0026	0.0028	0.0039
91.3	B_T	0.1193	0.0002	0.0007	0.0033	0.0039	0.0052
91.3	B_W	0.1201	0.0001	0.0014	0.0010	0.0021	0.0027
91.3	C	0.1188	0.0002	0.0009	0.0032	0.0035	0.0048
91.3	y_{23}^D	0.1202	0.0002	0.0025	0.0005	0.0019	0.0032
133.1	$1-T$	0.1126	0.0043	0.0038	0.0026	0.0032	0.0071
133.1	M_H	0.1110	0.0043	0.0033	0.0003	0.0020	0.0058
133.1	B_T	0.1065	0.0038	0.0048	0.0024	0.0027	0.0071
133.1	B_W	0.1123	0.0040	0.0026	0.0010	0.0017	0.0052
133.1	C	0.1051	0.0046	0.0029	0.0033	0.0024	0.0068
133.1	y_{23}^D	0.1071	0.0056	0.0053	0.0014	0.0012	0.0079
177.4	$1-T$	0.1088	0.0029	0.0027	0.0013	0.0028	0.0050
177.4	M_H	0.1081	0.0028	0.0042	0.0011	0.0018	0.0055
177.4	B_T	0.1051	0.0023	0.0031	0.0024	0.0026	0.0052
177.4	B_W	0.1047	0.0024	0.0029	0.0013	0.0012	0.0042
177.4	C	0.1067	0.0028	0.0030	0.0015	0.0025	0.0050
177.4	y_{23}^D	0.1084	0.0041	0.0031	0.0005	0.0013	0.0053
197.0	$1-T$	0.1109	0.0012	0.0019	0.0011	0.0030	0.0039
197.0	M_H	0.1075	0.0012	0.0021	0.0016	0.0018	0.0034
197.0	B_T	0.1092	0.0011	0.0019	0.0013	0.0029	0.0039
197.0	B_W	0.1069	0.0011	0.0011	0.0004	0.0013	0.0021
197.0	C	0.1086	0.0013	0.0017	0.0016	0.0026	0.0037
197.0	y_{23}^D	0.1073	0.0019	0.0023	0.0003	0.0013	0.0033

Table 4: Measurements of α_S using NNLO predictions and event shape distributions at 91.3 GeV. The employed covariance matrix includes an estimate of the experimental systematic covariance. The statistical error is taken from the fit with only the statistical covariance. The experimental systematic uncertainty is given by the fit error with quadratically subtracted statistical uncertainty.

Obs.	α_S(91.3 GeV)	$\pm$stat.	$\pm$exp.	χ^2/d.o.f.
$1-T$	0.1168	0.0002	0.0007	111/5
M_H	0.1291	0.0002	0.0027	18.3/4
B_T	0.1247	0.0002	0.0011	311/5
B_W	0.1107	0.0001	0.0009	142/4
C	0.1177	0.0002	0.0012	45.0/4
y_{23}^D	0.1183	0.0002	0.0010	1.6/3

Table 5: Measurements of α_S using NNLO+NLLA predictions and event shape distributions in four ranges of c.m. energy: at 91.3 GeV, 133.1 GeV, 161–183 GeV (177.4 GeV on average) and 189–209 GeV (197.0 GeV on average).

$\sqrt{s}$ [GeV]	Obs.	$\alpha_S(\sqrt{s})$	±stat.	±exp.	±had.	±theo.	±tot.
91.3	$1-T$	0.1219	0.0002	0.0012	0.0030	0.0041	0.0052
91.3	M_H	0.1207	0.0002	0.0008	0.0022	0.0033	0.0041
91.3	B_T	0.1213	0.0002	0.0010	0.0023	0.0048	0.0054
91.3	B_W	0.1164	0.0001	0.0013	0.0011	0.0041	0.0044
91.3	C	0.1186	0.0002	0.0009	0.0030	0.0046	0.0056
91.3	y_{23}^D	0.1195	0.0002	0.0025	0.0004	0.0023	0.0034
133.1	$1-T$	0.1128	0.0044	0.0040	0.0025	0.0032	0.0072
133.1	M_H	0.1094	0.0042	0.0029	0.0003	0.0023	0.0056
133.1	B_T	0.1085	0.0041	0.0055	0.0016	0.0034	0.0078
133.1	B_W	0.1082	0.0035	0.0028	0.0013	0.0033	0.0057
133.1	C	0.1049	0.0047	0.0034	0.0027	0.0030	0.0071
133.1	y_{23}^D	0.1068	0.0056	0.0051	0.0012	0.0017	0.0079
177.4	$1-T$	0.1089	0.0029	0.0028	0.0012	0.0027	0.0050
177.4	M_H	0.1069	0.0027	0.0039	0.0013	0.0021	0.0053
177.4	B_T	0.1070	0.0026	0.0034	0.0019	0.0032	0.0057
177.4	B_W	0.1018	0.0023	0.0026	0.0012	0.0027	0.0046
177.4	C	0.1063	0.0029	0.0031	0.0014	0.0030	0.0054
177.4	y_{23}^D	0.1079	0.0040	0.0031	0.0005	0.0016	0.0053
197.0	$1-T$	0.1110	0.0013	0.0020	0.0012	0.0029	0.0039
197.0	M_H	0.1064	0.0012	0.0021	0.0017	0.0021	0.0036
197.0	B_T	0.1112	0.0012	0.0021	0.0011	0.0035	0.0044
197.0	B_W	0.1045	0.0010	0.0013	0.0004	0.0029	0.0034
197.0	C	0.1083	0.0013	0.0019	0.0017	0.0032	0.0043
197.0	y_{23}^D	0.1068	0.0019	0.0022	0.0003	0.0016	0.0033

Table 6: Measurements of α_S using NNLO+NLLA predictions and event shape distributions at 91.3 GeV. The employed covariance matrix includes an estimate of the experimental systematic covariance. The statistical error is taken from the fit with only the statistical covariance. The experimental systematic uncertainty is given by the fit error with quadratically subtracted statistical uncertainty.

Obs.	$\alpha_S(91.3 \text{ GeV})$	$\pm$stat.	$\pm$exp.	χ^2/d.o.f.
$1-T$	0.1216	0.0002	0.0008	17.0/5
M_H	0.1215	0.0002	0.0021	2.6/4
B_T	0.1224	0.0002	0.0009	6.1/5
B_W	0.1145	0.0001	0.0010	3.4/4
C	0.1183	0.0002	0.0012	4.7/4
y_{23}^D	0.1191	0.0002	0.0011	0.3/3

Table 7: Combined values of $\alpha_S(\sqrt{s})$ at the OPAL c.m. energy ranges from NNLO (upper section) and NNLO+NLLA (lower section) analyses together with the statistical, experimental, hadronisation, theory and total uncertainties.

$\sqrt{s}$ [GeV]	$\alpha_S(\sqrt{s})$	$\pm$stat.	$\pm$exp.	$\pm$had.	$\pm$theo.	$\pm$tot.
			NNLO			
91.3	0.1205	0.0001	0.0011	0.0016	0.0027	0.0033
133.1	0.1109	0.0036	0.0027	0.0011	0.0022	0.0051
177.4	0.1057	0.0022	0.0027	0.0013	0.0020	0.0042
197.0	0.1077	0.0010	0.0012	0.0006	0.0018	0.0025
			NNLO+NLLA			
91.3	0.1196	0.0002	0.0012	0.0013	0.0036	0.0040
133.1	0.1088	0.0036	0.0029	0.0009	0.0030	0.0056
177.4	0.1042	0.0024	0.0027	0.0009	0.0027	0.0046
197.0	0.1069	0.0010	0.0016	0.0008	0.0029	0.0036

Table 8: Combined values of $\alpha_S(m_{Z^0})$ at OPAL c.m. energy ranges from NNLO (upper section) and NNLO+NLLA (lower section) analyses together with the statistical, experimental, hadronisation, theory and total uncertainties.

$\sqrt{s}$[GeV]	$\alpha_S(m_{Z^0})$	±stat.	±exp.	±had.	±theo.	±tot.
		NNLO				
130.1—206.6	0.1200	0.0012	0.0016	0.0008	0.0023	0.0032
91.3—206.6	0.1201	0.0008	0.0013	0.0010	0.0024	0.0031
		NNLO+NLLA				
130.1—206.6	0.1186	0.0011	0.0020	0.0009	0.0036	0.0040
91.3—206.6	0.1189	0.0008	0.0016	0.0010	0.0036	0.0041

Table 9: Combined values of $\alpha_S(m_{Z^0})$ for each observable from NNLO (upper section) and NNLO+NLLA (lower section) analyses together with the statistical, experimental, hadronisation, theory and total uncertainties.

Obs.	$\alpha_S(m_{Z^0})$	±stat.	±exp.	±had.	±theo.	±tot.
		NNLO				
$1-T$	0.1230	0.0010	0.0019	0.0018	0.0039	0.0048
M_H	0.1212	0.0009	0.0017	0.0020	0.0025	0.0037
B_T	0.1205	0.0009	0.0018	0.0016	0.0037	0.0045
B_W	0.1195	0.0009	0.0012	0.0007	0.0018	0.0024
C	0.1199	0.0011	0.0016	0.0023	0.0033	0.0045
y_{23}^D	0.1199	0.0008	0.0026	0.0004	0.0018	0.0033
		NNLO+NLLA				
$1-T$	0.1230	0.0010	0.0020	0.0020	0.0038	0.0048
M_H	0.1194	0.0009	0.0017	0.0020	0.0029	0.0040
B_T	0.1227	0.0009	0.0020	0.0016	0.0045	0.0053
B_W	0.1159	0.0009	0.0015	0.0007	0.0037	0.0042
C	0.1196	0.0011	0.0019	0.0023	0.0042	0.0053
y_{23}^D	0.1192	0.0010	0.0026	0.0004	0.0021	0.0035

23
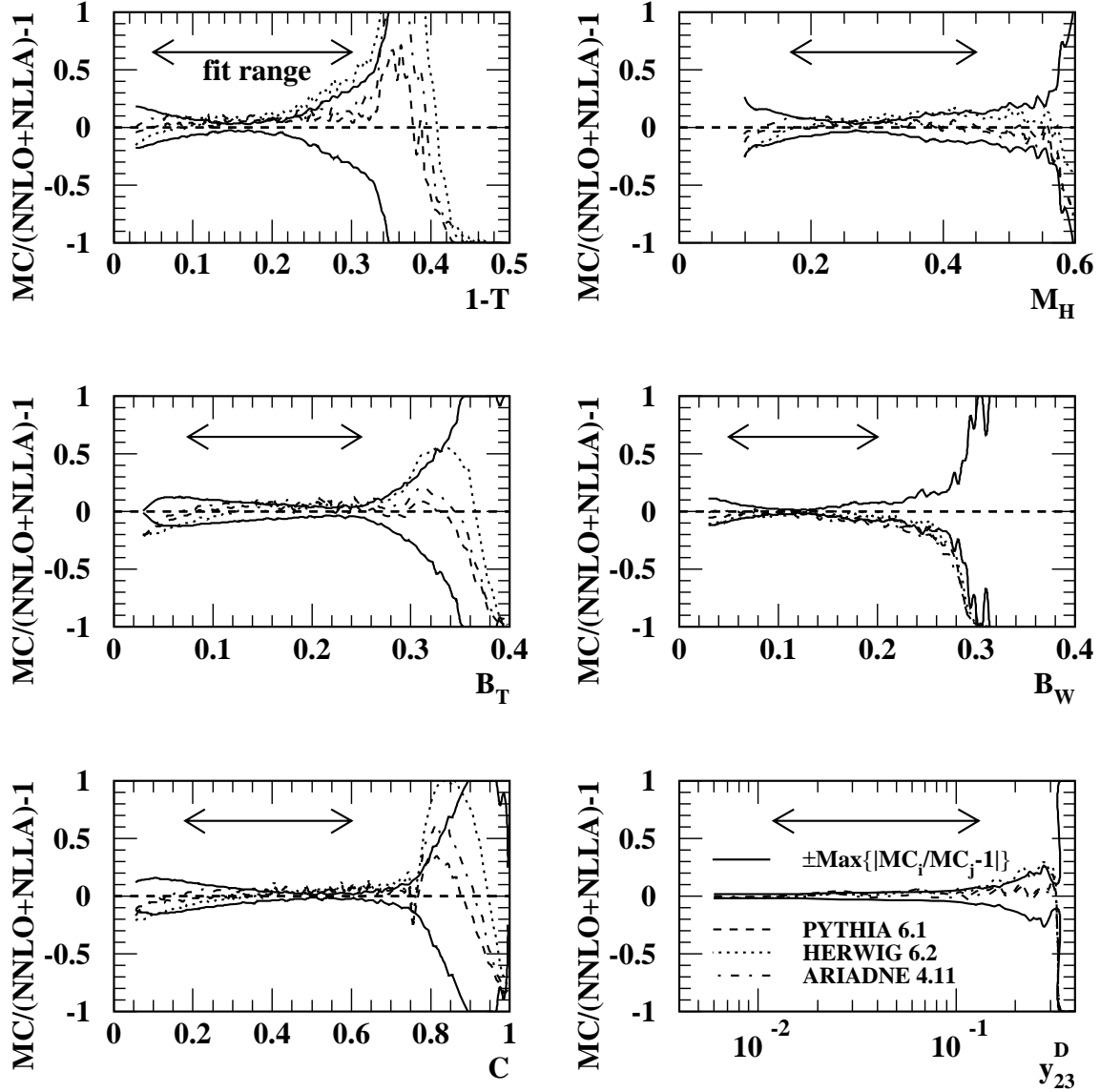
Figure 1: Comparison of NNLO+NLLA calculations for the $1 - T$, M_H, B_T, B_W, C and y_{23}^D variables with the parton level predictions of the Monte Carlo generators PYTHIA 6.1, HERWIG 6.2 and ARIADNE 4.11 at $\sqrt{s}$=91 GeV (see Sect. 6.1). The vertically symmetrical band between solid lines shows the maximum deviation of the ratio from one, between the three generators MC_i in the positive and the negative direction. The arrows indicate the respective fit ranges.

24
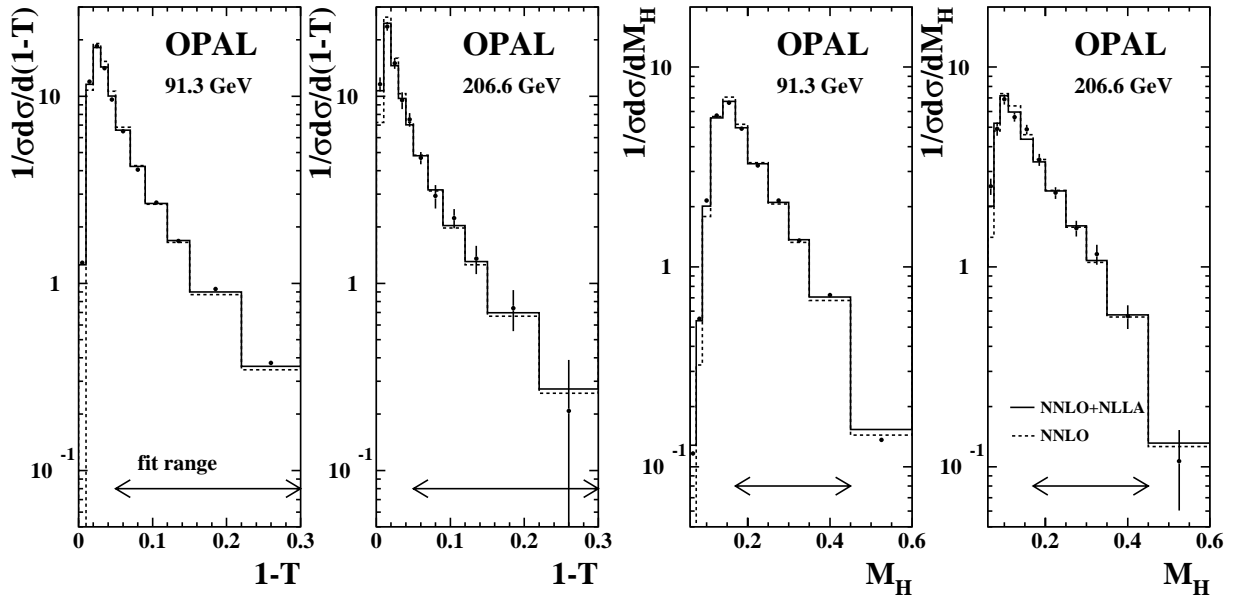
Figure 2: The points show the $1 - T$ and M_H distributions at the hadron level for $\sqrt{s} =$ 91.3 and 206.6 GeV with statistical uncertainty bars. Some uncertainty bars are smaller than the data points. Superimposed as histograms are the NNLO and NNLO+NLLA predictions combined with hadronisation effects using the corresponding fit results for $\alpha_S(\sqrt{s})$ shown in Tabs. 3, 5. The arrows indicate the fit ranges.
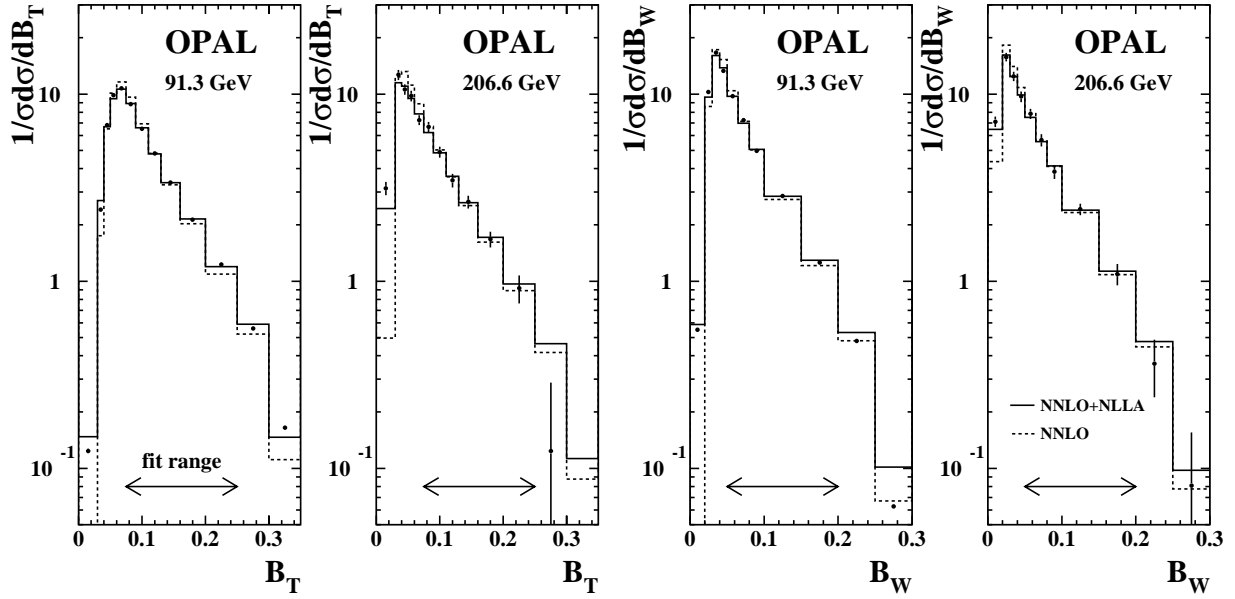
Figure 3: The points show the B_T and B_W distributions at the hadron level for $\sqrt{s} =$ 91.3 and 206.6 GeV with statistical uncertainty bars. Some uncertainty bars are smaller than the data points. Superimposed as histograms are the NNLO and NNLO+NLLA predictions combined with hadronisation effects using the corresponding fit results for $\alpha_S(\sqrt{s})$ shown in Tabs. 3, 5. The arrows indicate the fit ranges.
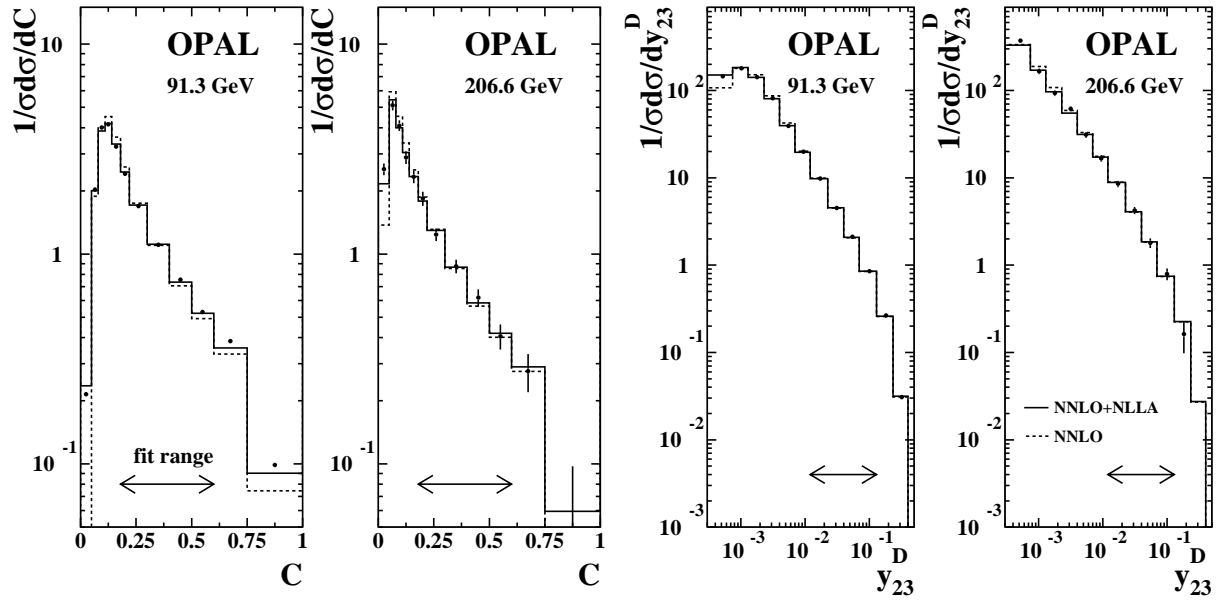
Figure 4: The points show the C and y_{23}^{D} distributions at the hadron level for $\sqrt{s} = 91.3$ and 206.6 GeV with statistical uncertainty bars. Some uncertainty bars are smaller than the data points. Superimposed as histograms are the NNLO and NNLO+NLLA predictions combined with hadronisation effects using the corresponding fit results for $\alpha_{\mathrm{S}}(\sqrt{s})$ shown in Tabs. 3, 5. The arrows indicate the fit ranges.

26
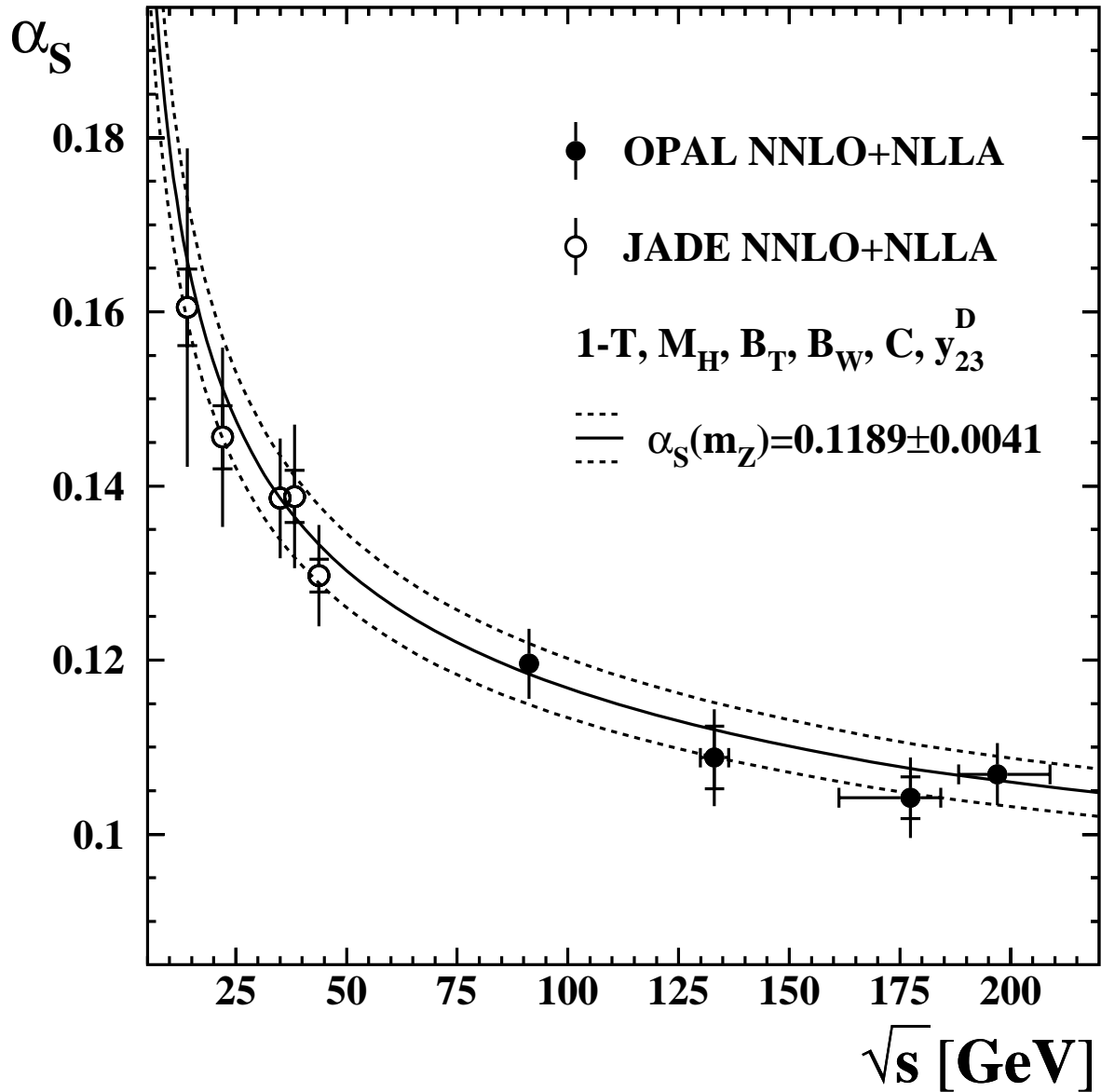
Figure 5: The points show the values of α_S for the OPAL energy ranges. The inner uncertainty bars show the combined statistical and experimental uncertainties and the outer the total uncertainties. The full and dashed lines indicate the α_S result from the NNLO+NLLA analysis that combines all variables and OPAL energy points. The results from the NNLO+NLLA analysis of JADE data [12] are shown as well.

27
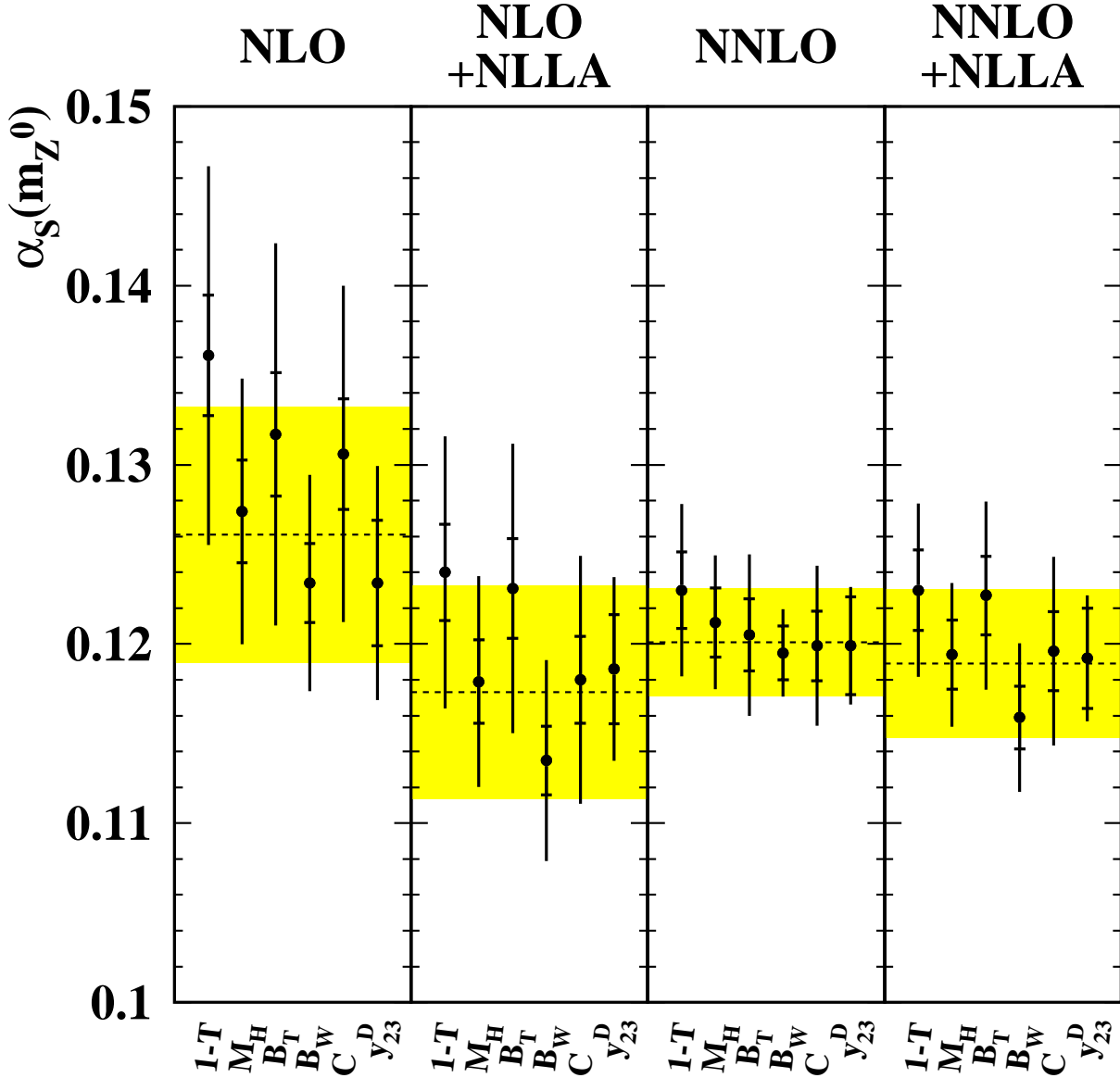
Figure 6: α_S results combined over all OPAL c.m. energies for different event shape variables and different QCD calculations as indicated on the figure. The shaded bands and dashed lines show the values of $\alpha_S(m_{Z^0})$ combined from these values with total uncertainties. The inner and outer uncertainty bars show the combined statistical and experimental and total uncertainties, respectively.
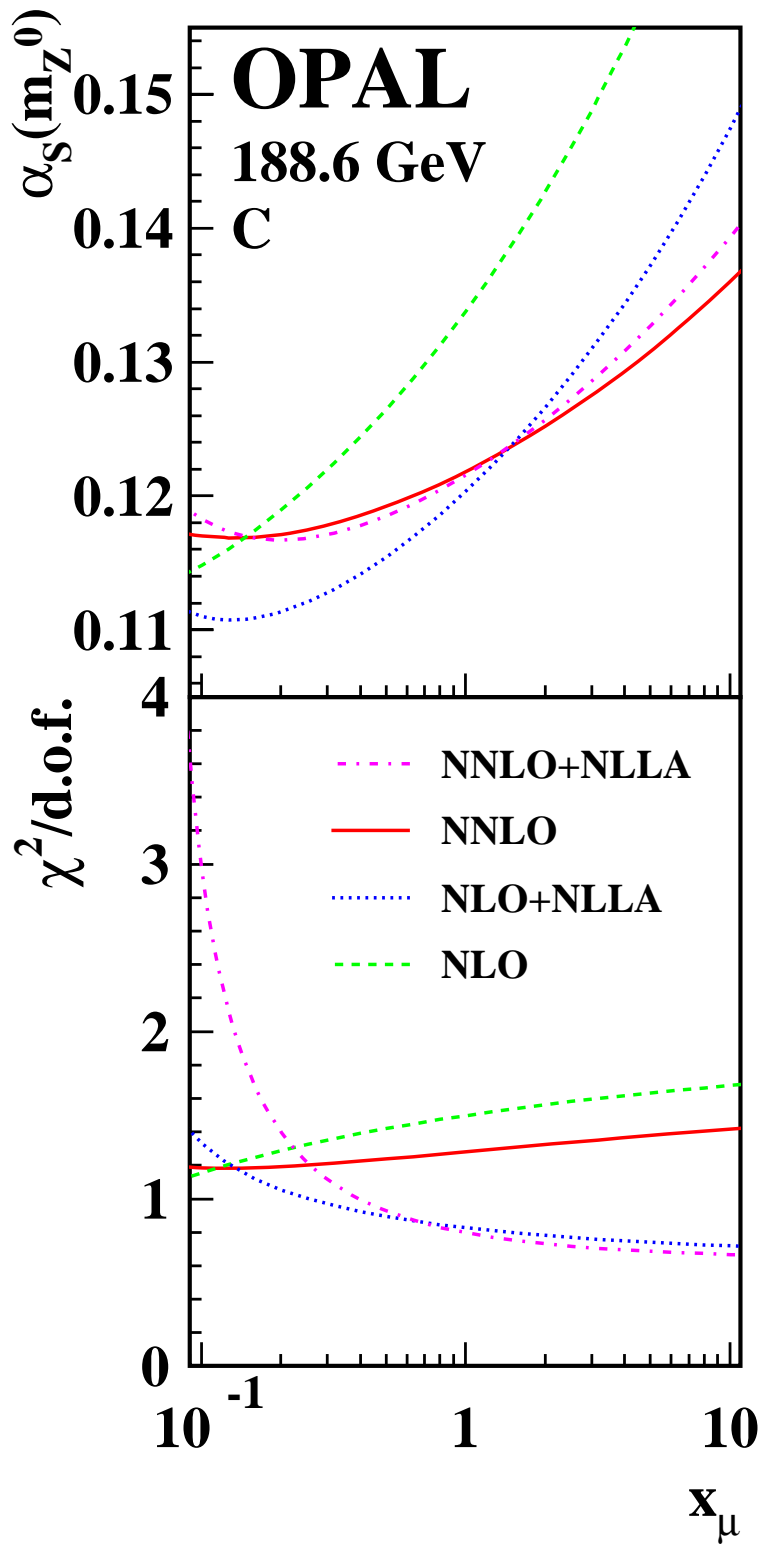
Figure 7: Results for α_S and χ^2/d.o.f. for fits of QCD predictions to the C distribution, as a function of x_μ.

A Appendix: Detailed results

Table 10: Results of NNLO fits to event shape observable distributions at the OPAL c.m. energies. The χ^2/d.o.f. values are based on the statistical errors only.

$\sqrt{s}$ [GeV]	Obs.	$\alpha_{\mathrm{S}}(\sqrt{s})$	$\pm$stat.	$\pm$exp.	$\pm$had.	$\pm$theo.	χ^2/d.o.f.
91.3	$1-T$	0.1220	0.0002	0.0011	0.0030	0.0042	440.1/5
91.3	M_{H}	0.1228	0.0002	0.0008	0.0027	0.0028	393.8/4
91.3	B_{T}	0.1193	0.0001	0.0007	0.0033	0.0039	1142.4/5
91.3	B_{W}	0.1201	0.0001	0.0013	0.0010	0.0021	446.6/4
91.3	C	0.1188	0.0002	0.0009	0.0032	0.0035	531.8/4
91.3	y_{23}^{D}	0.1202	0.0002	0.0025	0.0005	0.0019	31.5/3
130.1	$1-T$	0.1179	0.0057	0.0030	0.0025	0.0037	8.3/5
130.1	M_{H}	0.1158	0.0057	0.0027	0.0004	0.0023	6.5/4
130.1	B_{T}	0.1098	0.0051	0.0045	0.0019	0.0029	8.2/5
130.1	B_{W}	0.1155	0.0049	0.0020	0.0006	0.0018	0.8/4
130.1	C	0.1106	0.0061	0.0019	0.0028	0.0027	7.8/4
130.1	y_{23}^{D}	0.1106	0.0075	0.0046	0.0016	0.0014	4.7/3
136.1	$1-T$	0.1019	0.0062	0.0080	0.0029	0.0022	12.0/5
136.1	M_{H}	0.1012	0.0061	0.0067	0.0016	0.0014	5.1/4
136.1	B_{T}	0.1002	0.0053	0.0072	0.0034	0.0023	8.7/5
136.1	B_{W}	0.1021	0.0051	0.0082	0.0024	0.0013	7.0/4
136.1	C	0.0932	0.0065	0.0073	0.0045	0.0016	10.6/4
136.1	y_{23}^{D}	0.0999	0.0076	0.0095	0.0009	0.0010	3.0/3
161.3	$1-T$	0.1068	0.0065	0.0031	0.0025	0.0026	6.4/5
161.3	M_{H}	0.1073	0.0064	0.0040	0.0009	0.0017	3.9/4
161.3	B_{T}	0.1001	0.0055	0.0040	0.0034	0.0022	8.7/5
161.3	B_{W}	0.1022	0.0054	0.0023	0.0034	0.0012	9.4/4
161.3	C	0.1019	0.0066	0.0044	0.0034	0.0021	8.2/4
161.3	y_{23}^{D}	0.1060	0.0086	0.0020	0.0008	0.0013	2.0/3
172.1	$1-T$	0.1087	0.0076	0.0072	0.0030	0.0029	6.3/5
172.1	M_{H}	0.1068	0.0073	0.0062	0.0009	0.0018	5.0/4
172.1	B_{T}	0.1018	0.0064	0.0047	0.0021	0.0023	4.5/5
172.1	B_{W}	0.1001	0.0064	0.0039	0.0007	0.0011	1.9/4
172.1	C	0.1046	0.0075	0.0071	0.0033	0.0024	7.0/4
172.1	y_{23}^{D}	0.1044	0.0104	0.0132	0.0013	0.0012	2.6/3
182.7	$1-T$	0.1098	0.0035	0.0025	0.0018	0.0029	0.6/5
182.7	M_{H}	0.1091	0.0033	0.0044	0.0015	0.0018	4.4/4
182.7	B_{T}	0.1078	0.0028	0.0029	0.0021	0.0028	9.0/5
182.7	B_{W}	0.1071	0.0029	0.0032	0.0005	0.0013	4.3/4
182.7	C	0.1086	0.0034	0.0026	0.0018	0.0026	1.1/4
182.7	y_{23}^{D}	0.1103	0.0048	0.0040	0.0003	0.0014	1.4/3

Table 11: Results of NNLO fits to event shape observable distributions at the OPAL c.m. energies. The χ^2/d.o.f. values are based on the statistical errors only.

$\sqrt{s}$ [GeV]	Obs.	$\alpha_S(\sqrt{s})$	±stat.	±exp.	±had.	±theo.	χ^2/d.o.f.
188.6	$1-T$	0.1133	0.0020	0.0015	0.0014	0.0032	14.3/5
188.6	$M_{\rm H}$	0.1090	0.0020	0.0021	0.0018	0.0018	4.9/4
188.6	$B_{\rm T}$	0.1100	0.0017	0.0013	0.0011	0.0030	5.0/5
188.6	$B_{\rm W}$	0.1074	0.0017	0.0006	0.0006	0.0014	2.1/4
188.6	C	0.1094	0.0021	0.0012	0.0016	0.0027	6.4/4
188.6	$y_{23}^{\rm D}$	0.1083	0.0029	0.0020	0.0004	0.0013	3.5/3
191.6	$1-T$	0.1112	0.0050	0.0085	0.0017	0.0031	1.9/5
191.6	$M_{\rm H}$	0.1094	0.0048	0.0055	0.0014	0.0019	4.1/4
191.6	$B_{\rm T}$	0.1015	0.0046	0.0089	0.0025	0.0022	10.2/5
191.6	$B_{\rm W}$	0.1044	0.0042	0.0050	0.0005	0.0013	0.8/4
191.6	C	0.1053	0.0053	0.0060	0.0020	0.0024	0.3/4
191.6	$y_{23}^{\rm D}$	0.1051	0.0071	0.0066	0.0005	0.0012	0.0/3
195.5	$1-T$	0.1119	0.0033	0.0040	0.0021	0.0031	9.6/5
195.5	$M_{\rm H}$	0.1057	0.0033	0.0032	0.0018	0.0016	2.0/4
195.5	$B_{\rm T}$	0.1081	0.0029	0.0026	0.0016	0.0028	6.7/5
195.5	$B_{\rm W}$	0.1062	0.0029	0.0018	0.0007	0.0013	4.5/4
195.5	C	0.1087	0.0035	0.0035	0.0017	0.0026	1.9/4
195.5	$y_{23}^{\rm D}$	0.1008	0.0048	0.0046	0.0004	0.0010	1.4/3
199.5	$1-T$	0.1105	0.0034	0.0057	0.0021	0.0029	8.5/5
199.5	$M_{\rm H}$	0.1061	0.0034	0.0028	0.0007	0.0017	7.1/4
199.5	$B_{\rm T}$	0.1102	0.0030	0.0039	0.0023	0.0030	8.5/5
199.5	$B_{\rm W}$	0.1076	0.0029	0.0020	0.0010	0.0013	3.9/4
199.5	C	0.1077	0.0036	0.0039	0.0012	0.0026	5.5/4
199.5	$y_{23}^{\rm D}$	0.1130	0.0049	0.0045	0.0009	0.0015	4.8/3
201.6	$1-T$	0.1168	0.0048	0.0051	0.0013	0.0035	1.5/5
201.6	$M_{\rm H}$	0.1045	0.0049	0.0047	0.0012	0.0016	12.2/4
201.6	$B_{\rm T}$	0.1072	0.0044	0.0027	0.0015	0.0027	8.4/5
201.6	$B_{\rm W}$	0.1057	0.0043	0.0026	0.0017	0.0012	7.7/4
201.6	C	0.1092	0.0052	0.0061	0.0024	0.0026	11.3/4
201.6	$y_{23}^{\rm D}$	0.1107	0.0071	0.0076	0.0008	0.0014	1.4/3
204.9	$1-T$	0.1111	0.0032	0.0032	0.0015	0.0031	8.7/5
204.9	$M_{\rm H}$	0.1134	0.0029	0.0036	0.0006	0.0021	7.0/4
204.9	$B_{\rm T}$	0.1091	0.0028	0.0057	0.0011	0.0029	4.7/5
204.9	$B_{\rm W}$	0.1108	0.0027	0.0034	0.0005	0.0015	3.1/4
204.9	C	0.1085	0.0033	0.0068	0.0017	0.0027	3.3/4
204.9	$y_{23}^{\rm D}$	0.1090	0.0045	0.0060	0.0007	0.0013	3.7/3
206.6	$1-T$	0.1066	0.0026	0.0019	0.0018	0.0026	2.9/5
206.6	$M_{\rm H}$	0.1055	0.0025	0.0017	0.0021	0.0016	0.8/4
206.6	$B_{\rm T}$	0.1100	0.0021	0.0027	0.0010	0.0030	0.8/5
206.6	$B_{\rm W}$	0.1061	0.0022	0.0024	0.0006	0.0013	0.9/4
206.6	C	0.1079	0.0026	0.0020	0.0017	0.0026	1.6/4
206.6	$y_{23}^{\rm D}$	0.1058	0.0037	0.0026	0.0003	0.0012	0.6/3

Table 12: Results of NNLO+NLLA fits to event shape observable distributions at the OPAL c.m. energies. The $\chi^2/$d.o.f. values are based on the statistical errors only.

$\sqrt{s}$ [GeV]	Obs.	$\alpha_{\mathrm{S}}(\sqrt{s})$	$\pm$stat.	$\pm$exp.	$\pm$had.	$\pm$theo.	$\chi^2/$d.o.f.
91.3	$1-T$	0.1219	0.0002	0.0012	0.0030	0.0041	120.5/5
91.3	M_{H}	0.1206	0.0002	0.0008	0.0022	0.0033	66.8/4
91.3	B_{T}	0.1213	0.0002	0.0009	0.0023	0.0048	40.0/5
91.3	B_{W}	0.1164	0.0001	0.0013	0.0011	0.0041	108.9/4
91.3	C	0.1187	0.0002	0.0009	0.0030	0.0046	51.2/4
91.3	y_{23}^{D}	0.1195	0.0002	0.0025	0.0005	0.0023	8.0/3
130.1	$1-T$	0.1178	0.0058	0.0031	0.0025	0.0037	8.1/5
130.1	M_{H}	0.1138	0.0054	0.0022	0.0008	0.0026	6.7/4
130.1	B_{T}	0.1130	0.0056	0.0050	0.0024	0.0039	5.5/5
130.1	B_{W}	0.1119	0.0046	0.0019	0.0009	0.0036	1.0/4
130.1	C	0.1113	0.0063	0.0024	0.0019	0.0038	6.4/4
130.1	y_{23}^{D}	0.1105	0.0075	0.0044	0.0015	0.0019	4.4/3
136.1	$1-T$	0.1026	0.0063	0.0084	0.0025	0.0023	11.0/5
136.1	M_{H}	0.1003	0.0059	0.0066	0.0018	0.0017	4.7/4
136.1	B_{T}	0.1012	0.0056	0.0079	0.0034	0.0026	8.2/5
136.1	B_{W}	0.0993	0.0047	0.0076	0.0024	0.0024	7.3/4
136.1	C	0.0927	0.0064	0.0073	0.0044	0.0016	10.5/4
136.1	y_{23}^{D}	0.0996	0.0075	0.0093	0.0008	0.0012	2.9/3
161.3	$1-T$	0.1076	0.0066	0.0032	0.0020	0.0028	5.6/5
161.3	M_{H}	0.1068	0.0062	0.0037	0.0017	0.0022	3.1/4
161.3	B_{T}	0.1021	0.0059	0.0041	0.0029	0.0027	7.5/5
161.3	B_{W}	0.1001	0.0051	0.0022	0.0030	0.0025	9.1/4
161.3	C	0.1024	0.0067	0.0046	0.0029	0.0028	7.4/4
161.3	y_{23}^{D}	0.1057	0.0085	0.0020	0.0007	0.0015	1.9/3
172.1	$1-T$	0.1080	0.0076	0.0071	0.0032	0.0024	6.7/5
172.1	M_{H}	0.1047	0.0069	0.0057	0.0015	0.0019	5.6/4
172.1	B_{T}	0.1038	0.0069	0.0054	0.0015	0.0029	3.7/5
172.1	B_{W}	0.0978	0.0060	0.0038	0.0007	0.0023	2.0/4
172.1	C	0.1038	0.0075	0.0072	0.0034	0.0025	7.2/4
172.1	y_{23}^{D}	0.1038	0.0102	0.0129	0.0013	0.0015	2.6/3
182.7	$1-T$	0.1098	0.0035	0.0026	0.0018	0.0028	0.4/5
182.7	M_{H}	0.1080	0.0032	0.0040	0.0017	0.0022	3.7/4
182.7	B_{T}	0.1102	0.0031	0.0032	0.0015	0.0035	5.5/5
182.7	B_{W}	0.1047	0.0027	0.0030	0.0004	0.0029	3.5/4
182.7	C	0.1083	0.0035	0.0028	0.0019	0.0032	0.6/4
182.7	y_{23}^{D}	0.1098	0.0047	0.0039	0.0003	0.0017	1.3/3

Table 13: Results of NNLO+NLLA fits to event shape observable distributions at the OPAL c.m. energies. The χ^2/d.o.f. values are based on the statistical errors only.

$\sqrt{s}$ [GeV]	Obs.	$\alpha_S(\sqrt{s})$	$\pm$stat.	$\pm$exp.	$\pm$had.	$\pm$theo.	χ^2/d.o.f.
188.6	$1-T$	0.1133	0.0020	0.0016	0.0012	0.0032	13.6/5
188.6	M_{H}	0.1077	0.0019	0.0020	0.0019	0.0021	4.3/4
188.6	B_{T}	0.1119	0.0019	0.0014	0.0012	0.0036	2.1/5
188.6	B_{W}	0.1048	0.0016	0.0006	0.0006	0.0029	1.1/4
188.6	C	0.1092	0.0021	0.0014	0.0018	0.0033	4.0/4
188.6	y_{23}^{D}	0.1077	0.0028	0.0020	0.0004	0.0016	3.6/3
191.6	$1-T$	0.1110	0.0051	0.0085	0.0016	0.0028	2.1/5
191.6	M_{H}	0.1076	0.0046	0.0055	0.0011	0.0021	4.8/4
191.6	B_{T}	0.1040	0.0050	0.0099	0.0021	0.0028	7.9/5
191.6	B_{W}	0.1019	0.0040	0.0049	0.0005	0.0026	0.9/4
191.6	C	0.1047	0.0053	0.0060	0.0020	0.0027	0.3/4
191.6	y_{23}^{D}	0.1046	0.0070	0.0066	0.0005	0.0014	0.0/3
195.5	$1-T$	0.1121	0.0034	0.0041	0.0020	0.0031	9.0/5
195.5	M_{H}	0.1047	0.0032	0.0032	0.0020	0.0020	1.2/4
195.5	B_{T}	0.1104	0.0032	0.0028	0.0012	0.0035	3.9/5
195.5	B_{W}	0.1038	0.0027	0.0017	0.0005	0.0028	3.7/4
195.5	C	0.1083	0.0036	0.0034	0.0018	0.0031	1.6/4
195.5	y_{23}^{D}	0.1005	0.0047	0.0046	0.0003	0.0013	1.2/3
199.5	$1-T$	0.1109	0.0035	0.0059	0.0017	0.0031	7.2/5
199.5	M_{H}	0.1052	0.0033	0.0029	0.0010	0.0020	6.0/4
199.5	B_{T}	0.1129	0.0034	0.0045	0.0019	0.0039	4.9/5
199.5	B_{W}	0.1053	0.0028	0.0020	0.0006	0.0029	2.5/4
199.5	C	0.1077	0.0037	0.0040	0.0013	0.0032	4.2/4
199.5	y_{23}^{D}	0.1124	0.0048	0.0044	0.0009	0.0019	4.9/3
201.6	$1-T$	0.1172	0.0049	0.0053	0.0010	0.0037	1.0/5
201.6	M_{H}	0.1036	0.0048	0.0047	0.0010	0.0019	11.7/4
201.6	B_{T}	0.1097	0.0048	0.0036	0.0011	0.0034	6.5/5
201.6	B_{W}	0.1035	0.0041	0.0025	0.0013	0.0028	7.1/4
201.6	C	0.1104	0.0054	0.0068	0.0020	0.0038	9.3/4
201.6	y_{23}^{D}	0.1104	0.0070	0.0074	0.0007	0.0018	1.2/3
204.9	$1-T$	0.1108	0.0032	0.0031	0.0014	0.0028	9.9/5
204.9	M_{H}	0.1117	0.0029	0.0034	0.0005	0.0024	7.9/4
204.9	B_{T}	0.1108	0.0030	0.0060	0.0011	0.0034	4.5/5
204.9	B_{W}	0.1077	0.0025	0.0032	0.0004	0.0032	4.7/4
204.9	C	0.1081	0.0033	0.0070	0.0017	0.0031	3.3/4
204.9	y_{23}^{D}	0.1085	0.0044	0.0060	0.0007	0.0017	3.5/3
206.6	$1-T$	0.1068	0.0027	0.0019	0.0021	0.0025	2.1/5
206.6	M_{H}	0.1042	0.0025	0.0017	0.0022	0.0019	0.7/4
206.6	B_{T}	0.1116	0.0023	0.0030	0.0012	0.0035	1.5/5
206.6	B_{W}	0.1035	0.0021	0.0022	0.0005	0.0028	1.4/4
206.6	C	0.1076	0.0027	0.0021	0.0018	0.0031	0.9/4
206.6	y_{23}^{D}	0.1054	0.0036	0.0025	0.0004	0.0015	0.5/3

Table 14: Results of NLO+NLLA fits to event shape observable distributions at the OPAL c.m. energies. The $\chi^2/\text{d.o.f.}$ values are based on the statistical errors only.

$\sqrt{s}$ [GeV]	Obs.	$\alpha_{\text{S}}(\sqrt{s})$	$\pm$stat.	$\pm$exp.	$\pm$had.	$\pm$theo.	$\chi^2/\text{d.o.f.}$
91.3	$1-T$	0.1233	0.0002	0.0012	0.0031	0.0073	247.1/5
91.3	M_{H}	0.1196	0.0002	0.0008	0.0020	0.0057	36.9/4
91.3	B_{T}	0.1226	0.0002	0.0009	0.0029	0.0076	190.5/5
91.3	B_{W}	0.1145	0.0001	0.0013	0.0012	0.0055	140.2/4
91.3	C	0.1173	0.0002	0.0009	0.0031	0.0064	144.3/4
91.3	y_{23}^{D}	0.1192	0.0002	0.0025	0.0005	0.0044	4.5/3
130.1	$1-T$	0.1187	0.0059	0.0032	0.0027	0.0065	8.6/5
130.1	M_{H}	0.1129	0.0054	0.0021	0.0008	0.0048	6.4/4
130.1	B_{T}	0.1138	0.0057	0.0050	0.0024	0.0063	5.8/5
130.1	B_{W}	0.1100	0.0046	0.0019	0.0010	0.0050	1.1/4
130.1	C	0.1100	0.0061	0.0023	0.0022	0.0054	6.8/4
130.1	y_{23}^{D}	0.1104	0.0074	0.0043	0.0014	0.0035	4.2/3
136.1	$1-T$	0.1031	0.0064	0.0085	0.0027	0.0044	11.6/5
136.1	M_{H}	0.0995	0.0058	0.0066	0.0018	0.0032	4.4/4
136.1	B_{T}	0.1017	0.0057	0.0079	0.0036	0.0048	8.7/5
136.1	B_{W}	0.0976	0.0047	0.0076	0.0024	0.0036	7.3/4
136.1	C	0.0919	0.0063	0.0071	0.0044	0.0030	10.6/4
136.1	y_{23}^{D}	0.0995	0.0075	0.0094	0.0008	0.0026	2.9/3
161.3	$1-T$	0.1083	0.0067	0.0032	0.0023	0.0051	5.9/5
161.3	M_{H}	0.1061	0.0062	0.0035	0.0019	0.0041	2.7/4
161.3	B_{T}	0.1026	0.0060	0.0041	0.0032	0.0049	7.8/5
161.3	B_{W}	0.0984	0.0051	0.0022	0.0029	0.0037	8.9/4
161.3	C	0.1012	0.0065	0.0045	0.0030	0.0042	7.7/4
161.3	y_{23}^{D}	0.1056	0.0085	0.0019	0.0006	0.0030	1.8/3
172.1	$1-T$	0.1090	0.0077	0.0073	0.0033	0.0050	6.6/5
172.1	M_{H}	0.1036	0.0069	0.0056	0.0016	0.0035	5.8/4
172.1	B_{T}	0.1045	0.0070	0.0054	0.0016	0.0051	3.7/5
172.1	B_{W}	0.0961	0.0060	0.0037	0.0007	0.0035	2.0/4
172.1	C	0.1029	0.0074	0.0070	0.0034	0.0042	7.2/4
172.1	y_{23}^{D}	0.1038	0.0102	0.0130	0.0012	0.0029	2.6/3
182.7	$1-T$	0.1108	0.0036	0.0026	0.0018	0.0053	0.6/5
182.7	M_{H}	0.1071	0.0032	0.0039	0.0018	0.0041	3.6/4
182.7	B_{T}	0.1110	0.0031	0.0033	0.0017	0.0059	6.0/5
182.7	B_{W}	0.1029	0.0027	0.0029	0.0004	0.0042	3.6/4
182.7	C	0.1073	0.0034	0.0027	0.0019	0.0049	0.6/4
182.7	y_{23}^{D}	0.1096	0.0047	0.0039	0.0003	0.0034	1.3/3

Table 15: Results of NLO+NLLA fits to event shape observable distributions at the OPAL c.m. energies. The χ^2/d.o.f. values are based on the statistical errors only.

$\sqrt{s}$ [GeV]	Obs.	$\alpha_{\mathrm{S}}(\sqrt{s})$	$\pm$stat.	$\pm$exp.	$\pm$had.	$\pm$theo.	χ^2/d.o.f.
188.6	$1-T$	0.1143	0.0021	0.0016	0.0014	0.0058	14.2/5
188.6	M_{H}	0.1068	0.0019	0.0020	0.0019	0.0040	4.1/4
188.6	B_{T}	0.1128	0.0019	0.0014	0.0012	0.0061	2.7/5
188.6	B_{W}	0.1031	0.0016	0.0006	0.0006	0.0042	1.2/4
188.6	C	0.1083	0.0021	0.0013	0.0018	0.0050	4.1/4
188.6	y_{23}^{D}	0.1075	0.0028	0.0020	0.0004	0.0032	3.4/3
191.6	$1-T$	0.1120	0.0052	0.0087	0.0016	0.0055	2.0/5
191.6	M_{H}	0.1067	0.0046	0.0055	0.0010	0.0039	5.0/4
191.6	B_{T}	0.1045	0.0051	0.0100	0.0024	0.0051	8.4/5
191.6	B_{W}	0.1002	0.0040	0.0048	0.0004	0.0039	0.9/4
191.6	C	0.1039	0.0053	0.0059	0.0020	0.0044	0.3/4
191.6	y_{23}^{D}	0.1044	0.0070	0.0066	0.0005	0.0030	0.0/3
195.5	$1-T$	0.1130	0.0034	0.0041	0.0021	0.0057	9.3/5
195.5	M_{H}	0.1040	0.0032	0.0032	0.0021	0.0038	0.8/4
195.5	B_{T}	0.1112	0.0032	0.0028	0.0013	0.0059	4.5/5
195.5	B_{W}	0.1021	0.0027	0.0017	0.0005	0.0041	3.7/4
195.5	C	0.1073	0.0035	0.0033	0.0018	0.0049	1.7/4
195.5	y_{23}^{D}	0.1003	0.0047	0.0046	0.0003	0.0026	1.2/3
199.5	$1-T$	0.1117	0.0036	0.0059	0.0020	0.0055	7.8/5
199.5	M_{H}	0.1045	0.0033	0.0029	0.0012	0.0039	5.2/4
199.5	B_{T}	0.1136	0.0034	0.0046	0.0022	0.0062	6.0/5
199.5	B_{W}	0.1036	0.0028	0.0019	0.0005	0.0042	2.2/4
199.5	C	0.1066	0.0036	0.0039	0.0013	0.0049	4.6/4
199.5	y_{23}^{D}	0.1121	0.0048	0.0043	0.0009	0.0037	4.8/3
201.6	$1-T$	0.1182	0.0050	0.0054	0.0011	0.0065	1.1/5
201.6	M_{H}	0.1029	0.0048	0.0048	0.0009	0.0036	11.4/4
201.6	B_{T}	0.1105	0.0049	0.0034	0.0011	0.0058	6.7/5
201.6	B_{W}	0.1018	0.0040	0.0025	0.0013	0.0040	7.1/4
201.6	C	0.1091	0.0053	0.0065	0.0020	0.0053	9.7/4
201.6	y_{23}^{D}	0.1102	0.0070	0.0073	0.0007	0.0035	1.2/3
204.9	$1-T$	0.1118	0.0032	0.0032	0.0014	0.0054	9.6/5
204.9	M_{H}	0.1109	0.0029	0.0034	0.0006	0.0045	7.9/4
204.9	B_{T}	0.1117	0.0031	0.0061	0.0011	0.0060	4.2/5
204.9	B_{W}	0.1059	0.0025	0.0031	0.0005	0.0045	5.2/4
204.9	C	0.1072	0.0032	0.0069	0.0017	0.0049	3.0/4
204.9	y_{23}^{D}	0.1084	0.0044	0.0060	0.0006	0.0033	3.4/3
206.6	$1-T$	0.1076	0.0027	0.0019	0.0020	0.0049	2.2/5
206.6	M_{H}	0.1034	0.0025	0.0017	0.0022	0.0036	0.8/4
206.6	B_{T}	0.1126	0.0024	0.0030	0.0012	0.0061	1.2/5
206.6	B_{W}	0.1018	0.0021	0.0022	0.0005	0.0040	1.5/4
206.6	C	0.1066	0.0026	0.0020	0.0018	0.0048	1.1/4
206.6	y_{23}^{D}	0.1052	0.0036	0.0025	0.0004	0.0030	0.5/3